

Probing surfaces with single-polymer atomic force microscope experiments

C. Friedsam

*DEAS and Department of Physics, Harvard University, Cambridge, Massachusetts 02138
and Center for Nanoscience, LMU München, Geschwister-Scholl Platz 1, 80799 München, Germany*

H. E. Gaub

Center for Nanoscience, LMU München, Geschwister-Scholl Platz 1, 80799 München, Germany

R. R. Netz^{a)}

Physik Department, TU München, 85748 Garching, Germany

(Received 18 November 2005; accepted 20 December 2005; published 4 April 2006)

In the past 15 years atomic force microscope (AFM) based force spectroscopy has become a versatile tool to study inter- and intramolecular interactions of single polymer molecules. Irreversible coupling of polymer molecules between the tip of an AFM cantilever and the substrate allows one to study the stretching response up to the high force regime of several nN. For polymers that glide or slip laterally over the surface with negligible friction, on the other hand, the measured force profiles exhibit plateaus which allow one to extract the polymer adsorption energies. Long-term stable polymer coatings of the AFM tips allow for the possibility of repeating desorption experiments from solid supports with individual molecules many times, yielding good sampling statistics and thus reliable estimates for adsorption energies. In combination with recent advances in theoretical modeling, a detailed picture of the conformational statistics, backbone elasticity, and the adsorption characteristics of single polymer molecules is obtained. © 2006 American Vacuum Society. [DOI: 10.1116/1.2171996]

I. INTRODUCTION

Polymers are long-chain molecules that consist of identical subunits. In the course of the last century they have evolved as standard materials for all types of commodities in everyday life as well as in industrial applications. In the past tens of years they have invaded new fields of applications, e.g., they have become a prominent material for surface modification and functionalization and for devices such as polymer-based lasers,¹ diodes,² or solar cells.³ They clearly play key roles in disciplines like nano- or biosciences. Due to their numerous applications in material science, biology, medicine, and engineering, it is not surprising that charged and neutral polymers are the focus of current basic and applied research.⁴⁻⁹

In line with their versatile applicability, strong emphasis is put on the mechanical properties of polymeric materials. Their mechanical stability makes them competitive to metallic materials even at high mechanical loads or high temperatures. This progress is promoted by the synthesis of types of polymers as well as by ways of processing. Recent approaches tend to mimic polymeric materials found in nature that stand out because of their extraordinary load capacity like sinews or cartilage.¹⁰ The mechanical characteristics of individual polymer chains are closely related to the macroscopic properties of polymeric materials. This accounts for such aspects as entropic and enthalpic elasticity or the mechanical stability of molecular bonds as well as for molecular conformations. The measured data of conventional ensemble measurements reflect the collective properties of the bulk

assembly. They neither allow the extraction of the properties of a single molecule nor the analysis of the different intramolecular and intramolecular contributions that determine the material behavior on the macroscopic scale.

Polyelectrolytes (PEs) are a subgroup of polymers carrying ionizable groups that dissociate in aqueous solution, giving rise to a charged polymer and solvated counterions. Their behavior is determined by the interplay of electrostatics and conformational entropy and is thus different from both neutral polymers and simple electrolyte solutions.^{4,7,9} Due to the very long range nature of the electrostatic interactions, they are more complex than neutral polymers and the traditional separation of scales, which promotes the understanding of uncharged polymers in terms of simple scaling arguments, often does not work. Thus the theoretical description of polyelectrolyte molecules is a special challenge and the fact that they are charged is the basis for some unique features, e.g., their very small overlap concentration and their high solution viscosity. This arises from the fact that polyelectrolyte molecules take up a much more extended conformation than neutral polymers which is due to the presence of long ranged electrostatic repulsion between their charged monomers. The presence of a large number of counterions close to the charged units increases the osmotic pressure of polyelectrolyte solutions making these polymers in general water soluble. This is one of the main reasons for their outstanding role in the context of industrial processes.^{4,6,7} In particular their interaction with solid supports is the basis of numerous applications such as mineral separation,¹¹ flocculation,^{12,13} or retention.¹⁴ Analogous to the situation in bulk solution, the origin of the special adsorption properties of polyelectrolytes arises from the interplay between electrostatic repulsion and

^{a)}Electronic mail: netz@ph.tum.de

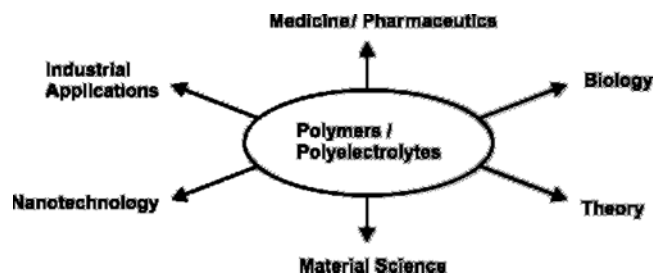


FIG. 1. Impact of polymer and polyelectrolyte research.

counterion degrees of freedom. Polyelectrolyte bulk and adsorption properties are also at the heart of many biological processes. One example is the growth of biominerals which is believed to be determined by specific interactions between biopolymers and mineral surfaces.^{15–18} Their widespread occurrence and importance make polyelectrolytes and polyelectrolyte adsorption in particular interesting for experimental research^{19–32} and for theoretical considerations.^{33–46} The impact of polyelectrolytes and polymers in general is illustrated in Fig. 1.

Stretching and desorption measurements of single molecules are a promising approach to enhance the understanding of polymers and their adsorption properties. Apart from this, such measurements open up the possibility for systematic investigations of different intermolecular interactions. Intermolecular interactions impact a variety of phenomena in material science, such as adhesion or friction.^{47,48} They also play a leading role in the fields of biology and life sciences, e.g., membrane assembly^{5,49–53} or protein folding.^{54–56} Particularly in biology weak noncovalent interactions, such as electrostatic, hydrogen bonding, or hydrophobic/hydrophilic interactions control essential processes.⁵ However, for synthetic polymeric materials they are also of crucial importance as they impact the mechanical stability of the fabricated materials. The ability to detect and interpret such intermolecular interactions under different environmental conditions provides the unique opportunity to gain deeper insight into the underlying mechanisms and derive a more detailed understanding of the processes at the molecular level.

II. SINGLE MOLECULE TECHNIQUES

A. Evolution and motivation

Thermodynamic and kinetic theory represent the traditional approach to determine interactions between macromolecules and macromolecular assemblies. Information about short range interactions between molecules is given by thermodynamic measurements such as pressure-volume-temperature data, boiling points, latent heats of vaporization, or lattice energies.^{57,58} Rheology, nuclear magnetic resonance, and x-ray as well as light/neutron scattering techniques provide information on short range interaction via macromolecular conformations and intermolecular correlations. A direct, macroscopic measurement of intermolecular interactions is realized by particle adhesion and peeling experiments, surface tension, and contact angle measurements

or the osmotic pressure technique.^{5,59,60} Although these techniques deliver valuable details concerning the interactions between molecules and molecular conformations, a lot of characteristic details are hidden in such a bulk measurement as they are based on averaging over large ensembles of molecules. Thus measurements at the single molecule level remained a goal, driven by the desire to learn more about the details that determine the mechanical properties of single molecules and single molecular bonds.

The most straightforward approach to measure forces between single molecules is to separate them and measure the binding force via the deflection of a spring attached to one of the particles. While this is a very simple principle for macroscopic particles, it is a very challenging task at the molecular level. The first striking breakthrough was the development of the surface force apparatus, which has a force resolution of approximately 10 nN and a vertical resolution of 0.1 nm.^{61–63} It allows us to measure the force law between two surfaces that are typically represented by two atomically smooth mica surfaces covered with the molecules under investigation. To perform measurements on the single molecule scale requires the possibility to exert minute forces at the pN scale, while at the same time distances at the range of nm have to be controlled. Thus it is not astonishing that progress in this field primarily relies on technical and instrumental evolution. In the past 20 years, experimental techniques were developed that made the pN as well as the fN range accessible. The most recent developments even allow us to probe the aN range.⁶⁴ A variety of techniques evolved that finally allowed measurements on the single molecule scale and investigations of inter- and intramolecular interaction in great detail and with a precision unknown before. The most prominent techniques differing in force and dynamic range are glass microneedles,⁶⁵ magnetic beads,^{66–68} atomic force microscopy (AFM),^{69–81} optical tweezers,^{82–86} hydrodynamic techniques,^{87–92} and the biomembrane probe.^{93,94}

B. Single molecule force spectroscopy

AFM-based single molecule force spectroscopy was one of the first single molecule techniques. Originally just one of the operational modes of atomic force microscopy, single molecule force spectroscopy has in the meantime emerged as a powerful technique, which allows the measurement of intra- and intermolecular forces with unparalleled precision and sensitivity.^{24,74,95–98} Originally its popularity was based on the fact that it allows the structural and functional investigation of single biomolecules in their native environment, but apart from this it has also become an established tool for the study of material properties and structures.^{99,100} The measured binding forces range from the pN regime, e.g., for receptor-ligand systems^{75,101,102} to the nN regime that is reached when single covalent bonds are ruptured.¹⁰³

Single molecule force spectroscopy has emerged from the study of single biomolecules.^{104–106} One of the early breakthroughs was the measurement of the binding force of a

single biotin–streptavidin complex.^{75,107} The manipulation of single biopolymers has led to fascinating new insights into the mechanics of, e.g., proteins and DNA at the molecular level.^{54,55,74,108–116} Single molecule force spectroscopy opened up a perspective to understand the folding of proteins including intermediate states.^{115,117–119} The stretching experiments of single DNA molecules revealed an overstretching transition in the moderate force regime and a force induced melting transition at higher forces^{108,120} and they also provide the perspective to study the effect of cancer drugs on DNA mechanics which could support therapeutical approaches.¹²¹ Thus single molecule force spectroscopy has promoted a rapidly growing knowledge about the relation between structure, function, and force.

While the early results, e.g., the measurements of the bond strength of individual receptor–ligand bonds,⁷⁵ tried to determine a static and universal binding force, it is now well accepted that bond breaking is a dynamic process.^{122,123} Due to the fact that any single bond has a finite lifetime and will thus break spontaneously on a certain time scale, the measured rupture force depends strongly on the force loading rate. This finding promoted the development of dynamic force spectroscopy which allows us to explore the inner world of ligand–receptor bonds and thus can reveal a detailed picture of the binding potential including inner barriers that are difficult or impossible to detect in assays of near equilibrium dissociation.^{120,124–139} But as the dynamic range of AFM force spectroscopy is limited, bonds with a lifetime that differ significantly from the measurement time show no loading rate dependence. This accounts, e.g., for covalent bonds that show a very slow dynamics or it can be found if single electrostatic bonds are investigated that break and rebind on a very fast time scale.

The latter interactions are typically found in desorption experiments of single polyelectrolyte molecules from solid supports. This type of experiment has only recently been introduced as a subject of investigation in single molecule force spectroscopy.^{28,140} In previous studies single molecule force spectroscopy measurements revealed valuable details on the adsorption process of single polyelectrolyte strands on charged substrates. For example, the loop size distribution of adsorbed chains at the interface could be determined²⁷ as well as the desorption forces needed for pulling the strands away from the substrate.^{27–29,140,141} The equilibrium desorption forces for weak polyelectrolytes adsorbed on negatively charged surfaces were found to be linearly dependent on the Debye screening length, the surface number charge density, and the line number charge density of the polyelectrolytes.^{28,29} Desorption measurements extend the spectrum of AFM force spectroscopy investigations to functional synthetic polymers. Much of the experimental and theoretical understanding found in biophysical research can be applied directly to synthetic materials and will hopefully lead to the development of materials and applications.

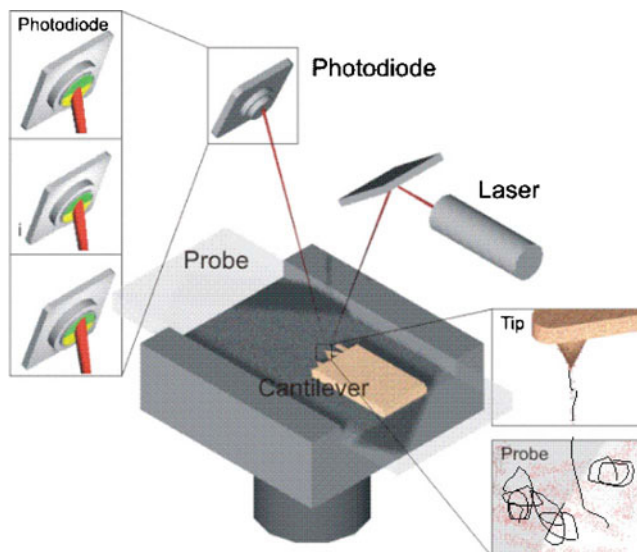


FIG. 2. Basic setup of an AFM: the force sensor is represented by a cantilever with a tip which is opposing the sample under investigation. As the radius of the tip is typically in the range of some tens of nm, it allows us to pick up single molecules. The force exerted on the cantilever is read out by a laser: the beam is focused on the cantilever and reflected to a segmented photodiode. As the cantilever is deflected, the spot of the reflected laser beam moves accordingly and the differential signal between the two segments changes.

III. EXPERIMENTAL DETAILS

A. AFM-based single molecule spectroscopy

AFM was introduced in 1986 by Binnig and Rohrer⁶⁹ as a high resolution tool for imaging.^{71,142–145} One of its further developments utilized the AFM as an experimental method for studying inter- and intramolecular interactions in surface-immobilized systems. The setup of the instrument is shown in Fig. 2: The force sensor is represented by a sharp tip (approximately 3 μm diameter and 50 nm radius of curvature) that is attached to a small cantilever. Typical values are 10–500 mN/m for the spring constant, 7–120 kHz for the resonance frequency in air, and 1–30 kHz in water. The vertical position of the cantilever can be varied by the movement of a piezoelectric crystal. Thus a mechanical force can be exerted on a single molecule or a single molecular bond that is clamped between the tip and the opposing surface. The exerted force is given by Hooke's law

$$F = kz_C, \quad (1)$$

where k means the spring constant of the cantilever and z_C its deflection which can be detected optically by the deflection of a laser beam focused on the cantilever and reflected to a segmented photodiode.

The differential voltage signal of the two-segment photodiode corresponds to the deflection of the cantilever. As a result a deflection-piezopath curve is recorded that can be converted in a force-extension curve reflecting the mechanical properties of the system under investigation. This procedure is illustrated in Fig. 3.

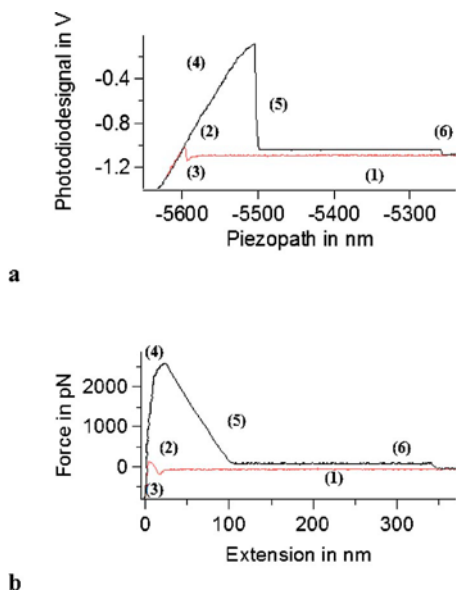


FIG. 3. Conversion of the deflection-piezopath curve to a force-extension curve (the light grey curve is measured when the cantilever is approaching the surface, the dark grey curve is obtained upon retraction of the cantilever). Points (1)–(6) mark specific parts of the measured data curve: (1) The cantilever is approaching the surface at zero force. (2) Snap into contact. (3) Indentation in the sample. (4) Unspecific adhesion. (5) Snap-off. (6) Complete desorption of a single polymer. (a) The raw data are obtained as photodiode (voltage) signal measuring the deflection of the cantilever against the piezopath. The measured piezopath does not equal the distance between the cantilever and the surface. This can be clearly seen when the cantilever is touching the surface which is indicated by the negative photodiode signal: although the distance should be constant the piezopath signal is changing, which is due to the fact that the deflection of the cantilever is not considered yet. For the same reason the photodiode signal snaps back to zero instantaneously when the molecule is ruptured. (b) If the indentation slope and the spring constant of the cantilever is known the original data can be converted to a force-extension curve. Now the distance is fixed at zero when the cantilever is touching the surface. Accordingly the force is decreasing to zero over a certain distance after the rupture of the molecule, reflecting the relaxation of the cantilever. The curve shown was recorded for polyacrylic acid that was adsorbed onto a CH_3 terminated self-assembled monolayer and the force loading rate was ≈ 5000 pN/s.

The raw data represent the difference signal between two segments of the photodiode plotted against the distance measured by the strain gauge. In order to come to the real distance that represents the extension of the attached molecule, the deflection of the cantilever has to be eliminated. To do so the slope of that part of the curve that represents the indentation of the cantilever on the substrate (in voltage/nm) has to be determined. Using this slope s , the distance z between the AFM tip and the surface is given by

$$z = a - s^{-1} \cdot \text{ph}_{a-b}, \quad (2)$$

where a means the piezopath in nm and ph_{a-b} the photodiode difference signal in Volts. In order to convert the difference signal into force, the spring constant of the cantilever has to be determined. This can be done by the analysis of the thermal oscillation spectrum of the cantilever: The spring constant k can be determined by integration over the ground oscillation in the power spectrum^{146,147} because the mean energy of the ground oscillation is given by $k_B T/2$ where k_B

means the Boltzmann constant and T the temperature. According to the equipartition theorem this gives the total energy stored on average in this degree of freedom:

$$\frac{k_B T}{2} = \frac{k \langle \Delta x^2 \rangle}{2}. \quad (3)$$

A small correction has to be made due to the laser geometry (represented by a factor of 0.8),¹⁴⁷ resulting in

$$k = \frac{0.8 k_B T}{\langle \Delta x^2 \rangle}. \quad (4)$$

The force F acting on the cantilever is then determined to be

$$F = k \cdot (z - a). \quad (5)$$

Plotting the force against the true cantilever-surface distance gives the force-extension profile for the investigated molecule. The different parts of the force-extension curve monitor various types of interactions between tip and surface: When the tip is approaching the surface, repulsive or attractive interactions can be observed. In the case of (long ranged) repulsive interactions a negative deflection of the cantilever is observed when the AFM tip is approaching the surface. If the interaction between tip and sample is attractive usually a snap-on is observed that is marked by a sudden jump of the force to positive values. The reason for this is a mechanical instability that occurs when the gradient of the force becomes equal to the spring constant of the cantilever.¹⁰⁵ The indentation part of the curve is marked by a negative force that is steadily rising. When the cantilever is retracted the force becomes positive again for an attractive tip-sample interaction. As the interaction of the tip with the surface can be very complex this part of the force-extension curve is usually referred to as “unspecific adhesion.” The end of this regime is usually marked by a sudden drop of the force corresponding to the “snap off” of the cantilever of the surface. Under the appropriate conditions single molecule events may be observed in the subsequent part of the force-extension curve. The snap-on and the snap-off of the curve hide certain parts of the force-extension curve that are thus inaccessible by experimental investigations. Dependent on the width of these regimes and the type of experiment this may be a serious problem. Strategies to prevent the unspecific interaction will be discussed later on.

The high sensitivity of a few picoNewton provides the necessary resolution to probe the response of individual molecules. The force resolution of the best instruments is only limited by thermal noise. The spatial resolution is in the sub-nm range. Until recently this was achieved by decoupling the z movement of the cantilever from the other directions by implementing manual xy translation.^{74,79,148} Newer instruments can also scan in three dimensions without loss in resolution due to the improved piezo technique. As will be shown the loading rate is also an important instrumental parameter. The AFM shows a lower limit of 10 pN/s which is due to thermal drift problems at lower loading rates. There is also an upper limit at 10^4 pN/s which is induced by the resonance frequency of the force transducer and viscous dis-

sipation when the cantilever is rapidly moved through the liquid. If the oscillation frequency of the AFM probe exceeds the resonance frequency of the force transducer, or if there is substantial viscous damping, the cantilever deflection will not reflect the true tip-sample interaction.^{77,149,150} To circumvent these limitations, smaller cantilevers have been developed with the same stiffness but smaller dimensions.¹⁵⁰ The smaller cantilevers minimize viscous damping and expand the frequency bandwidth accessible in the measurements by which the sensitivity of the force transducer is increased.

Further improvements include the implementation of a single-molecule force clamp, which allows AFM measurement under conditions of constant force¹⁵¹ and the combination with other experimental techniques, e.g., the combination of force spectroscopy and electrochemistry^{152–154} or the coupling of optical excitation into the AFM experiment.^{155,156}

B. Performance of the experiments

In the following we describe two extremal situations, namely the stretching case where the polymer sticks to the substrate and the polymer-substrate contact point is immobile, and the desorption case where the polymer slips over the substrate.

In a typical stretching experiment the polymer is immobilized on a substrate. After the sample is mounted onto the AFM the tip is brought into contact with the interfacial layer for some time to pick up one or several molecules. Depending on the nature of the tip-polymer interaction it will take several seconds up to minutes to achieve sufficient binding. Upon retraction, the deflection of the cantilever reflects the interaction between the tip and the functionalized surface. Very frequently unspecific interactions that result in strong adhesive forces are observed at short distances. As they represent a superposition of many different contributions including tip-substrate interactions, multiple molecular binding, desorption of polymer strands, etc., they are too complex to be analyzed. While this unspecific adhesion may be interesting in another context, it is highly undesirable for polymer stretching experiments because it hides interesting details of the stretching behavior in the low force regime. Sometimes the unspecific adhesion can be lowered by shortening the contact time (“fly fishing” of molecules) or by modifying the protocol of sample preparation, e.g., by coadsorbing substantially shorter polymer molecules onto the substrate that reduce the tip-substrate interaction. Other strategies are based on repeated cycles of retracting and approaching the surface while the distance to the substrate surface is slowly increased with the goal to get rid of shorter attached polymers and end up with a single molecule attached to the AFM tip. The force profile of this last remaining strand may then be taken repeatedly until rupture. The principal setup of this experiment is depicted in Fig. 4 left; a typical force extension curve is given in Fig. 4 right.

In the desorption experiments the polymers are grafted to the tip that is opposing a generic surface. When the tip is approaching the surface the polymer molecules are allowed

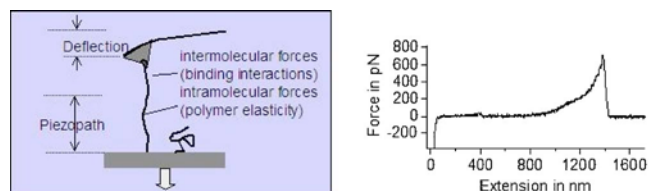


FIG. 4. Performance and typical force-extension curve for a stretching experiment: Typically the AFM tip is brought into contact with the sample, which is covered by a layer of polymer molecules (negative force indicates the indentation into the sample surface). If a molecule has bound to the tip it can be stretched and the force is measured via the deflection of the cantilever spring as a function of the extension. The force-extension curve, which corresponds to a single polymer molecule that is stretched upon retraction, shows a strongly nonlinear behavior. When the maximum binding force is exceeded, the molecule ruptures from the tip and the tip is free again. The force-extension curve shown here corresponds to a single polyacrylic acid molecule that is unspecifically bound to a gold coated tip.

to adsorb onto it. Upon retraction of the tip for distances of several hundreds of nanometers, the desorption process of one or multiple molecules from the surface is monitored. The most striking difference in the force extension curves of the desorption measurements compared to the polymer stretching curves, which will be discussed in more detail below, is that desorption plateaus at various force levels are recorded instead of spikes. The heights of the plateaus reflect the desorption force that is required to desorb one or multiple polymer molecules from the opposing surface, whereas the steps mark the desorption of one or more molecules with different adsorption lengths. The succession of measured forces in a desorption experiment is depicted in Fig. 5. The unspecific adhesion at short distances is a minor problem in this type of experiment but as the force shall be measured that is required to desorb one or more polymer molecules from the opposing generic surface it is important to ensure that the polymers are stably bound to the tip. If this is the case the attachment to the surface represents the weakest link that will break during the experiment so that the measured desorption force indeed reflects the desorption of the polymer molecule from the opposing surface.

Both types of experiments take place in solution. Depending on the type of experiment, specific environmental conditions like type or concentration of the salt in solution, solvent, substrate, etc. are varied and the response of the polymeric behavior is observed. It is at present not understood on a microscopic level what determines whether a specific polymer will be permanently attached on a certain substrate or whether it will glide under applied external force, but it is clear that the resulting friction behavior depends to a large degree on the effective friction coefficient between the polymer and the substrate.¹⁵⁷

C. Equilibrium and nonequilibrium measurements

The shape of the force extension curves in unbinding experiments of multiple bonds in series strongly depends on the dynamics of the system, ranging from saw-tooth like patterns to flat plateaus. This is supported by theory, suggesting that

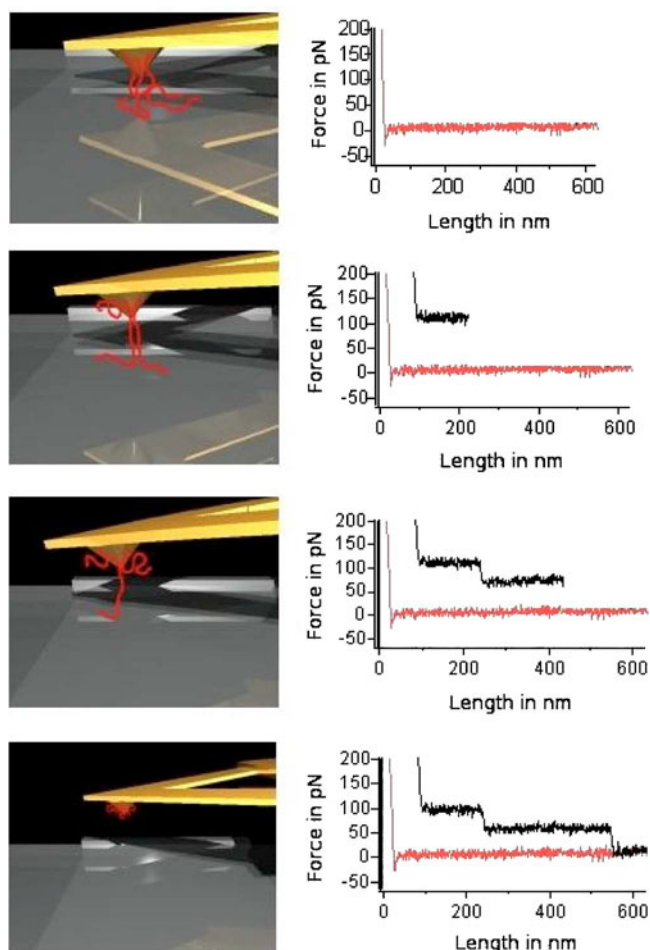


FIG. 5. Performance of a desorption experiment (polyacrylic acid grafted to a SAM-covered AFM tip adsorbed on a OH-SAM; details of functionalization and results are given below). When the cantilever is approaching the surface the AFM tip experiences an attractive force (indicated by the snap into contact) and the molecules are allowed to adsorb on the surface. Upon retraction of the AFM tip a high adsorption force is found at short distances which is composed of different multiple contributions. If the cantilever is retracted further a constant force is recorded which (in this case) reflects the desorption of two individual polymer molecules from the surface. When the shorter one is completely desorbed, the force drops and subsequently the desorption process of a single polymer molecule is recorded which shows a constant desorption force at a lower force level. Finally the second molecule is also detached, the force drops to zero, and the AFM tip is free again. In order to obtain significant statistics an appropriate quantity of adsorption-desorption cycles is recorded (typically 500–1000 force-extension curves).

the shape of the force-extension profiles for the desorption of polymer chains depends on the force loading rate.¹⁵⁸

Bond rupture forces are generally nonequilibrium or time-dependent values. They depend on the intrinsic lifetime of the bond, the temperature, and on the measurement time. On laboratory time scales the energy landscape along the dissociation pathway is explored by thermal excitations. Energy barriers produce a dissociation time that varies with applied force: On time scales longer than the natural lifetime for spontaneous thermally driven dissociation, an isolated single bond has no strength and will dissociate under zero force as there is a finite probability that it acquires sufficient thermal energy from its surrounding to overcome its activation bar-

rier. If a constant stretching force is applied along the bond axis, the intermolecular potential is effectively tilted by $-F \cdot (z - z_0)$. As a consequence the lifetime of the bond is shortened by the external force and the kinetic profile is transformed into a dynamic spectrum of bond rupture force as a function of loading rate. The force spectrum can be translated in an easy-to-read map that monitors the different energy barriers traversed along the force-driven pathway if it is depicted against the logarithm of the force loading rate. This accounts for covalent bonds, most of the specific receptor-ligand systems, as well as for the rupture of protein domains.

Two main reasons may be considered to explain the occurrence of desorption plateaus. If the polymer has a series of binding sites along its chain, the shape of the resulting force-extension curve depends strongly on the distance between two neighboring binding sites. With a decreasing distance between the ruptured bonds it becomes more difficult to resolve the single ruptures. Finally their overlay results in a plateau-like shape. In this case the measurements still take place in nonequilibrium. The height of the plateau is loading-rate dependent and therefore the observed histogram of the desorption forces is non-Gaussian. A second scenario for the occurrence of desorption plateaus involves kinetic arguments. If the bonds involved in the adsorption process dissociate and reassociate on a much faster time scale than the experimental pulling process occurs, no rupture events are observed. Instead a constant equilibrium desorption force is found that reflects the process of peeling off the polymer from the surface segment by segment. The measurement then takes place in thermal equilibrium; no loading rate dependence is observed and the investigated process is reversible. Therefore the histogram of the desorption forces is Gaussian. Continuous desorption plateaus are observed in experiments where the polymer is only very weakly adsorbed or bound via ionic bonds. The three described scenarios are illustrated in Fig. 6.

D. Data analysis

The scaling of different force extension traces can be utilized to separate the force extension curves that belong to the stretching of a single molecule from those that correspond to multiple polymer attachment: If the measured stretching force is a function of the relative extension of the polymer chain in the probed force regime, all force traces originating from individual polymer chains of different length but with identical structure should superimpose when scaled to the same contour length.

The possibility of identifying particular single polymers by polymer fits and scaling procedures is also very useful when the rupturing of single molecular bonds under nonequilibrium conditions is investigated. In this type of experiment polymers are usually used as spacers that allow the spatial separation of the interesting rupturing event from the unspecific adsorption at short distances. With the identification of specific single polymer stretching curves it is also possible to separate single bond ruptures that correspond to the investi-

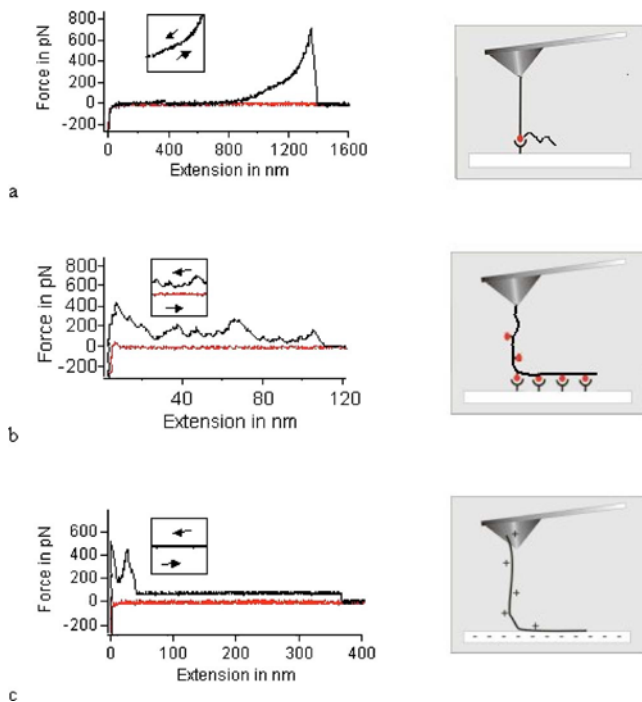


Fig. 6. Nonequilibrium and equilibrium measurements: Different shapes of force-extension curves and their schematic explanation (all force-extension curves were recorded for polyacrylic acid that was grafted to a gold coated AFM tip as described below and that was allowed to adsorb onto a gold surface with 5 mM NaCl in solution and varied pH). The insets show examples for reversible and irreversible processes. (a) pH 5: Stretching of a polymer that is mechanically stable coupled to the surface by one binding site as indicated in the picture on the right. The rupturing of this specific bond is a nonequilibrium process, as its natural lifetime is sufficiently high so that the bond remains closed during the whole pulling process. Thus the stretching of the polymer spacer is observed until the bond is ruptured by the applied force. The rupturing of the bond is an irreversible process, whereas the stretching of the polymer spacer is reversible: it is possible to go back and forth on the force curves and remeasure the stretching of the polymer without hysteresis. (b) pH 3: Rupturing of numerous bonds under nonequilibrium conditions. The polymer is coupled to the surface by numerous bonds as pictured on the right. The lifetime of each individual bond is high enough so that the stretching of the connecting polymer segments can be observed in principle. But when the distance between the different binding sites on the polymer becomes smaller and smaller it becomes more and more difficult to resolve the single rupture events and the force-extension curve is approaching a plateau-like shape. The rupturing of the bonds is an irreversible process. The surface has to be approached again at zero force in order to measure the rupturing of the bonds repeatedly. (c) pH 9: Desorption of a polymer molecule in an equilibrium process. The individual bonds dissociate and reassociate on a much faster time scale than the experimental pulling process occurs and the stretching of the polymer spacer can no longer be observed. Instead of this, one observes a desorption plateau whose height reflects the equilibrium desorption force required to peel the polymer off the surface segment by segment. The desorption of the polymer is a reversible process; it is possible to go back and forth on the desorption plateau. Such a situation is given when a polyelectrolyte molecule is bound to a charged surface by electrostatic interactions as they typically show a very high exchange rate. This scenario is depicted on the right side. It is at present not clear why the pH controls the desorption kinetics in such a decisive manner.

gated bond from dirt or multiple rupture events. The extracted rupture force histograms are usually broad non-Gaussian distributions.¹⁵⁹

If the on-off dynamics of individual bonds is much faster than the applicable stretching rates, desorption plateaus are

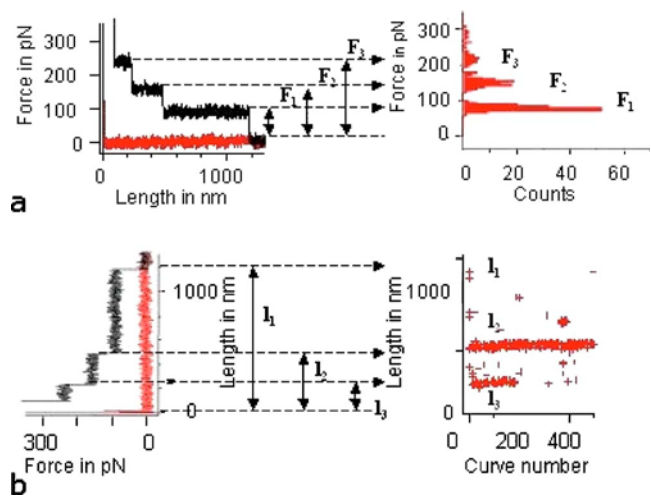


Fig. 7. Data and data analysis for equilibrium measurements: Analysis of the force-distance curves illustrated for the case where desorption plateaus were observed. If more than one step is observed, multiple molecules with different lengths are desorbed from the opposing surface upon retracting one after the other. (a) The height of the plateaus marks the desorption force that is required to desorb a single molecule or multiple polymer strands. The measured desorption force curves are collected in a histogram. Every step in the force-distance curve marks the point when a single molecule is completely desorbed. (b) The desorption lengths found in an individual force-distance curve are plotted against the number of the curve. In such a plot changes in the desorption lengths that accompany environmental changes can be illustrated.

measured instead of ruptures. The different steps represent the desorption of individual molecules of different lengths. Each time, when one polymer strand is completely desorbed a step in the desorption force is recorded until the last polymer is fully detached. The plateau length directly reflects the length of an adsorbed polymer, whereas the height of a plateau corresponds to the desorption force that is required to desorb one or multiple polymers from the opposing surface. The heights of the plateaus are collected in a desorption force histogram that shows—in contrast to the nonequilibrium case—one or more narrow Gaussian distributions as can be seen from Fig. 7(a). The peaks of these distributions represent the mean desorption force that is required to desorb one or more polyelectrolyte molecules from the opposing surface. As the polyelectrolyte molecules generally show broad length distributions that are hard to interpret, it is not favorable to collect the desorption lengths in a histogram. Instead of this the lengths of all desorption plateaus observed in a desorption experiment are plotted against their curve number. This process is illustrated in Fig. 7(b). In this type of depiction it is easier to correlate differences in the observed desorption lengths with changes in the environmental conditions.

E. Sample preparation

One of the most intriguing challenges of AFM force spectroscopy experiments is the preparation of the samples that can be in particular difficult when the molecules have to be coupled to the AFM tip. Generally three different types of methods are applied: physisorption, specific binding to sur-

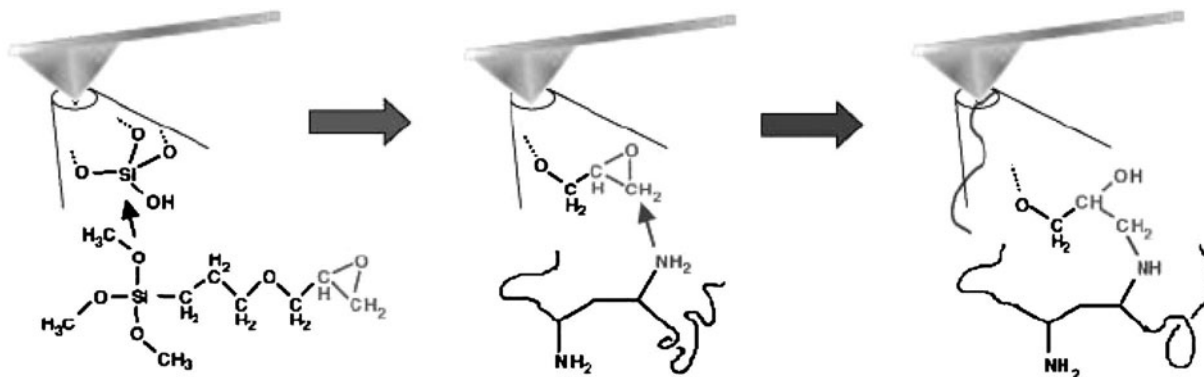


FIG. 8. Grafting by silanization (shown for epoxysilane coupled to polyvinylamine): The methoxyterminated epoxysilane is grafted to the Si_3N_4 AFM tip. The aminogroups of the polymer can bind to the epoxygroups of the silane. The final result is a PVA-coated AFM tip (cited from the literature, Ref. 29).

face groups, and covalent binding to surfaces. For many types of experiments it is sufficient if the molecules are unspecifically adsorbed either to the bare silicon nitride tip or to a gold coated tip during the experiment when the tip is indented into the polymer layer. This is the easiest and most straightforward way to bind the molecules to the tip. The unspecific binding of polymer chains to the tip was found to hold forces up to several hundred pN. This was suitable for a variety of polymer stretching experiments including the unfolding of proteins. But sometimes functional loss and structure changes that result from the close proximity of the investigated molecules to the surface raise a serious problem. This may be overcome if an intermediate layer of coupling molecules is introduced that binds the target molecules specifically.^{160,161} The most frequently used approaches are based on the use of receptor–ligand systems or metal–chelating complexes.^{162,163} One major problem with this type of functionalization is that these bonds typically show low yield forces, in particular at slow force-loading rates.¹²⁷ This problem may be solved if the molecules are covalently attached to the tip, as covalent bonds were found to hold up to several nN. The covalent attachment is absolutely necessary if covalent bonds themselves are the subject of investigation but it is also an important issue for polymer stretching experiments that focus on the high force regime. Most often primary amino groups, epoxy groups, free sulfhydryl groups, and carboxyl groups are used. Silanization has proven to be a suitable approach to functionalize the AFM tip with these reactive groups. Prominent examples are aminoterminated silanes that provide the possibility to bind carboxy groups via peptide bonds and epoxysilanes to which amino groups can be bound. The latter type of preparation is illustrated in Fig. 8.

The preparation and functionalization of long-term stable polymer coated AFM tips generally is also desirable for desorption measurements with single polyelectrolyte molecules as it provides the opportunity to measure a long series of desorption curves with one and the same set of molecules under various experimental conditions. The big advantage is that deviations due to different sample preparations can be ruled out this way and the results can be directly compared.

It includes in particular the possibility to probe several different surfaces with the same set of molecules. Thus the polyelectrolyte molecules can be utilized as high precision probes to characterize the properties of the different surfaces (see Fig. 9).

If the functionalized AFM tip is pushed on the surface many thousand times, several complications can be considered to limit the long-term stability of the polymer coating: the most important ones are detachment of the molecules from the tip, an increasing extent of unspecific binding to the tip, and contamination. These three scenarios and their consequences are illustrated in Fig. 10.

Although silanization was applied successfully in many cases^{102,103,164} aging and wearout of the silane layer were frequently found to limit the use of such tips in long-term measurements. A favorable alternative to silanization is the use of thiol chemistry on gold surfaces. In contrast to the silanization process on silicon nitride,^{165–168} it is less complicated to produce well-defined and densely packed monolay-

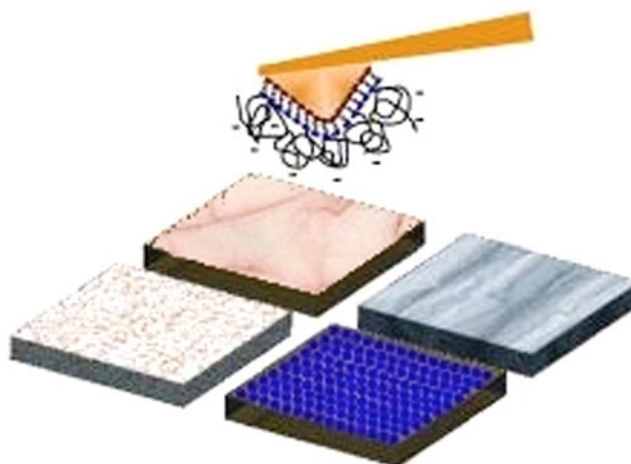


FIG. 9. Advantages of long-term measurements: Deviations due to different sample preparations can be ruled out and the adsorption behavior of the same set of polymer molecules can be observed with respect to different environmental conditions. In particular different surfaces can be probed and different surface characteristics can be determined at high precision.

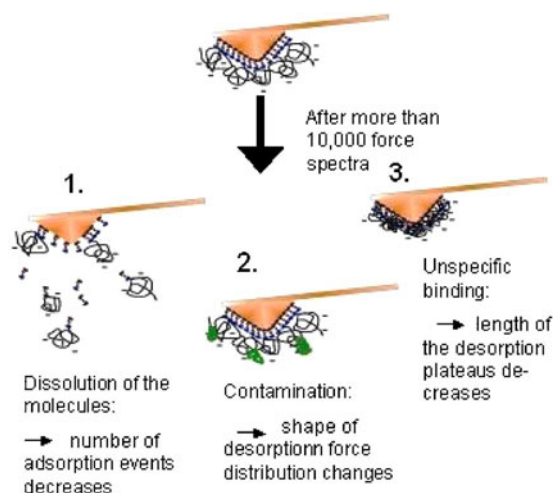


FIG. 10. Problems of long-term measurements: The long-term stability of a polymer coating can be limited for several reasons. The most important ones and the corresponding consequences observed in the course of an experiment are schematically depicted.

ers of mercapto-terminated alkyl chains on gold.^{169–172} This fact was utilized to remarkably enhance the long-term stability of functionalized AFM tips.¹⁷³ The technique could be successfully applied to bind polymers with carboxyl groups and polymers with amino groups via peptide bonds to an AFM tip, respectively. The whole process is illustrated in Fig. 11 for the case of polyacrylic acid.

For several reasons, desorption experiments themselves provide a suitable method to characterize the capability of the polymer coating to withstand long-term measurements. As the desorption processes are often found to be rate independent and thus show very narrow Gaussian force distributions, possible disturbances that would broaden these narrow distributions, e.g., from contaminations, can easily be identified. The adsorption-desorption process is mediated by a weak reversible binding process in this case and the corresponding desorption forces are 1 order of magnitude weaker than the covalent intramolecular bonds of the polymer. Consequently, the polymer structure is not affected by the desorption process. As a consequence, the general stability of the polymer coated tips with respect to environmental influences and aging could be monitored in such experiments. Concerning the long-term stability of the AFM tips three probable reasons for degradation and the related experimental consequences can be considered: (1) if one or several probe molecules would detach from the tip during the measurements, the number of adsorption events would decrease; (2) tip contamination would result in broad and undefined distributions of the desorption forces; and (3) if the molecules would form additional unspecific bonds to the AFM tip that are stronger than the bonds to the underlying substrate, the observed desorption length would decrease. The desorption length, the number of desorption events, and the shape of the desorption force histograms can therefore be used as criteria to exclude these degradation effects of the polymer coated tips. A typical example of such a long-term

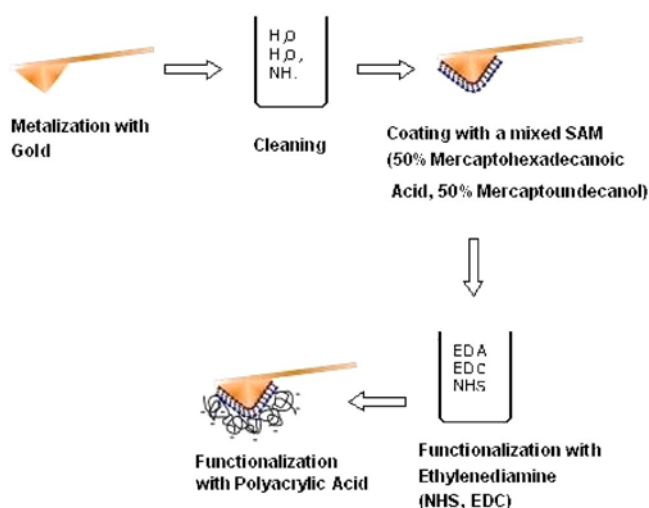


FIG. 11. SAM-based preparation of the AFM cantilever in the case of polyacrylic acid: first the AFM tip has to be coated with gold by thermal evaporation. The gold-coated tip is then cleaned in a solution of H_2O , H_2O_2 , and NH_3 (3:1:1) at $70^\circ C$. Then it is coated with a mixed SAM (50% COOH terminated, 50% OH terminated). The COOH-groups of the SAM are converted to NH_3 groups by ethylenediamine that is added in great excess. Finally the polyacrylic acid can be bound to the NH_3 groups at the tip via peptide bonds.

measurement is shown in Fig. 12. Figure 12(a) shows the desorption lengths for a polyacrylic acid coated tip probing various substrates (COOH, OH, CH_3 -SAM, gold, glass, calcite, mica) with $CaSO_4$ in solution. About 40 000 force spectra were recorded. For the measurement as a whole, no systematic decrease in desorption length could be observed. Thus it can be concluded that the polymer coating remains stable and no significant unspecific binding to the tip occurred during the measurement. In Fig. 12(b) the development of the desorption forces corresponding to the measurements shown in Fig. 12(a) is plotted. Three desorption force histograms are extracted: one at the beginning, one in the middle, and one at the end of the measurements. In each case 500 force spectra contribute to the desorption force histogram. Every histogram shows a narrow Gaussian peak that corresponds to the desorption of a single polymer chain from the probed substrate. Occasionally, additional peaks at higher forces appear which belong to the desorption of two or more polymer strands in parallel. As the distributions remain narrow and well defined during the whole measurement, the occurrence of significant contaminations can be excluded. As can also be seen from Fig. 12 the number of adsorption events remains constant during the entire experiment. This means that even after 40 000 force spectra the polymers remained stably attached to the tip.

The procedure is applicable for amino as well as for carboxyl groups. The polyelectrolytes that were successfully grafted to the tip by this method are illustrated in Fig. 13.

IV. DESORPTION OF SINGLE POLYMERS

The behavior of polyelectrolyte molecules differs significantly from that of neutral polymers due to the fact that

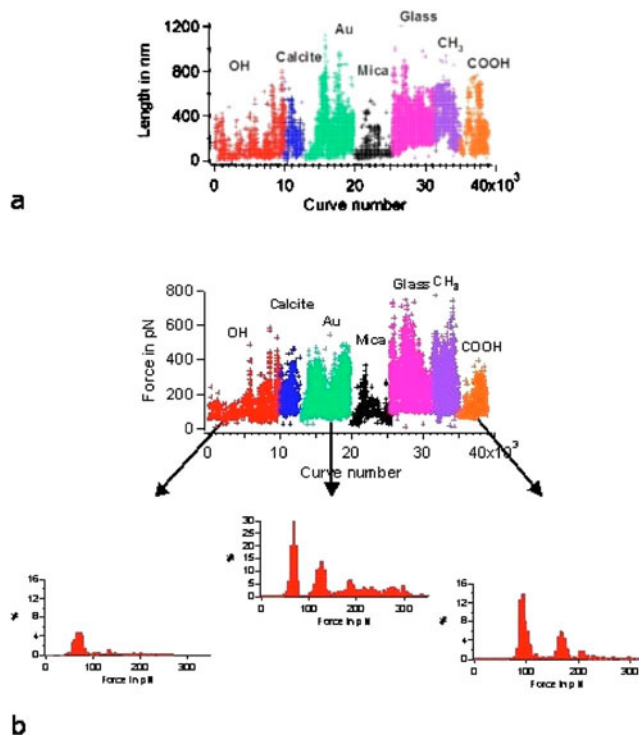


FIG. 12. Long-term stability of the polymer coating: Measurement with polyacrylic acid under various environmental conditions. (Top graph) The desorption lengths which are given by the lengths of the measured desorption plateaus are plotted against their curve number. During the whole measurement no systematic degradation could be observed. The second graph shows the measured desorption forces for the different samples and three different histograms that were extracted exemplarily at the beginning, in the middle and at the end of the measurement. The first histogram belongs to a measurement on a OH-SAM (0.5 mM CaSO_4 , pH 6), the second one to a measurement on gold (5 mM CaSO_4 , pH 3), and the last one to a measurement on the COOH-SAM (0.5 mM CaSO_4 , pH 6). In all three cases well-defined histograms were obtained. The number of desorption events is fluctuating strongly when the substrate is changed; but no decreasing tendency in the course of time can be observed.

polyelectrolytes become charged upon dissociation and display electrostatic interactions. Technically this is important because charges induce solubility in water which is one of the main reasons for the widespread use of polyelectrolytes in applications. Another important property is that they can adsorb on charged surfaces via electrostatic interactions. This is interesting on the one hand because of the numerous applications that are based on polyelectrolyte adsorption on interfaces but also because there are many ways to influence the strength of the electrostatic contribution to the adsorption energy as will be shown below. Several theoretical treatments exist that have been worked out to describe polyelectrolyte desorption from solid supports.^{23–29}

In a first very simplified approach the desorption force is described by the sum of an electrostatic contribution F_{el} , a constant nonelectrostatic contribution F_0 , and an entropic contribution accounting for chain compression/stretching in the adsorbed/nonadsorbed polymer sections, F_{en} (to be discussed later): $F_{\text{des}} = F_0 + F_{\text{en}} + F_{\text{el}}$. This approach is valid for a strongly adsorbed polymer, i.e., far from the desorption transition. If the involved electrostatic energies are of the order

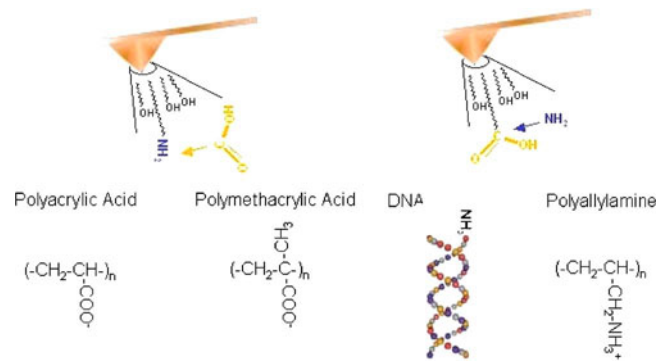


FIG. 13. Overview of the molecules which could be grafted by the technique described.

of several $k_B T$, the electrostatic contribution $F_{\text{el}} = \alpha\psi/a$ can be described as a product of the electrostatic surface potential $\psi/k_B T = 4\pi l_B \sigma \kappa^{-1} e^{-d\kappa}$, the fraction of charged monomers α , and the inverse monomer separation $1/a$. This leads to

$$F_{\text{des}} = F_0 + F_{\text{en}} + 4\pi l_B k_B T \sigma \kappa^{-1} e^{-d\kappa} \alpha / a, \quad (6)$$

where σ is the surface number charge density of the substrate, κ^{-1} the Debye screening length, $l_B = e^2 / (4\pi\epsilon k_B T)$ the Bjerrum length (i.e., the distance at which two unit charges interact with $k_B T$), and d is the surface distance of bound PE monomers. As the electrostatic contribution to F_{des} is proportional to κ^{-1} , the nonelectrostatic part can be determined by varying the salt concentration c_s and linear extrapolation $\kappa^{-1} = (8\pi l_B c_s)^{-1/2} \rightarrow 0$. Thus Eq. (6) can easily be probed by force spectroscopy experiments. In a first preliminary analysis the entropic contribution F_{en} is neglected, the surface distance d of bound PE monomers is assumed to be zero, and the line charge density $\tau = \alpha/a$ is regarded as a fixed value which leads to the simplified equation

$$F_{\text{des}} = F_0 + 4\pi l_B k_B T \sigma \kappa^{-1} \tau. \quad (7)$$

According to this equation the electrostatic adsorption force depends on three parameters: the charge density of the surface σ , the line charge density of the polyelectrolyte molecule τ , and the Debye screening length κ^{-1} that determines the range of the electrostatic interactions. Whereas the line charge density is fixed for strong polyelectrolytes it depends on the solution pH for weak polyelectrolytes. The Debye screening length depends on the salt concentration in solution and thus can easily be varied *in situ*. The surface number charge density can be varied by exchanging the substrate or by applying an external potential in the case of a conducting substrate. The different possibilities for modeling the strength of the electrostatic contribution to the adsorption force are depicted in Fig. 14.

One of the early AFM-based desorption studies dealt with the adsorption characteristics of PVA on glass.²⁸ In this publication the linear dependence on the Debye screening length as well as the linear dependence of the desorption force on the line charge density could be validated. The latter was possible because three different types of molecules were available. Each of them had a different proportion of charged

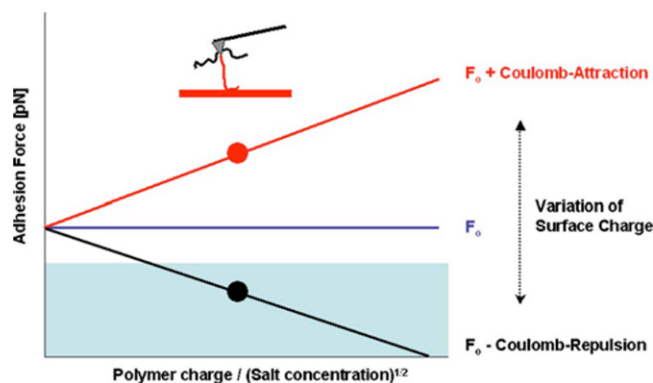


FIG. 14. Possibilities to influence the electrostatic contribution to the desorption force: while the electrostatic contribution can be diminished by increasing the salt concentration or reducing the line charge density of the polyelectrolyte molecule, the variation of the surface charge of the substrate even allows us to switch the sign of the electrostatic interaction from attractive to repulsive or vice versa.

side groups because a certain part of the amino groups was replaced by uncharged keto groups. The mean desorption forces for one single poly (vinyl alcohol) (PVA) chain was determined by analyzing the first peak in the histogram of the desorption forces for a certain NaCl concentration and a certain line charge density, respectively. These desorption forces were then plotted against their Debye screening length and their line charge density, respectively. The desorption force was found to be linearly increasing with the Debye screening length. This indicates an attractive force that is more and more screened when the NaCl concentration is increased. The desorption force was also found to be increasing with the line charge density of the polymer, supporting the results found for the screening length. Later on the studies with PVA were extended to other negatively charged surfaces, namely calcite and mica,^{20–22} basically confirming the results obtained for glass. For all substrates an estimate of the surface number charge density was given utilizing Eq. (7). Thus it could be shown that single polyelectrolyte molecules can be utilized as local probes to characterize certain surface properties.

So far only attractive electrostatic interactions were probed. The perspective was widened when the negatively charged polyacrylic acid became a subject of investigation. Repulsive electrostatic interactions could also be probed and additional results could be obtained to refine the picture.²⁹ Whereas the measurements with polyacrylic acid (PAA) on glass and NaCl in solution showed a more complicated behavior, the measurements on calcite gave qualitatively the expected results for a varied NaCl concentration in solution and could easily be compared to the results obtained with PVA: in the case of PAA the desorption force was found to be decreasing with the Debye screening length indicating a repulsive interaction. The results for both polymers are shown in Fig. 15. It is striking that the absolute value of the slopes is not the same for both polymers, indicating that the model used represents an oversimplification. This fact will be discussed in more detail below.

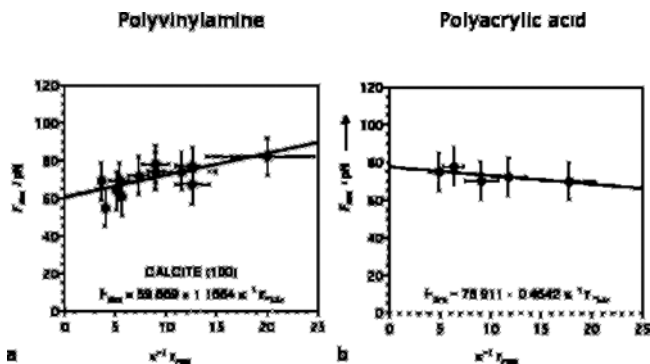


FIG. 15. Adhesion forces of polyvinylamine and polyacrylic acid to calcite(104). Their linear dependence on $\kappa^{-1}\tau_{\max}$ reveals attractive and repulsive Coulombic interactions for: (a) cationic PVA and (b) anionic PAA, respectively.

If the same desorption experiment is done with mica,²⁹ which represents a stronger negatively charged surface than calcite, no adhesion of the negatively charged polyacrylic acid was observed with NaCl in solution. Only under strong screening conditions ($c_{\text{NaCl}}=100$ mM) will short range attractions between the polyacrylic acid coated AFM tip and the mica surface be observed, but no long desorption plateaus, which would represent the desorption of a single polyacrylic chain, were found. This fact is due to the stronger electrostatic repulsion that could not be sufficiently screened by the salt in solution.

If the measurements were done with CaSO_4 in solution even small salt concentrations (0.5 mM) could enable the adsorption of polyacrylic acid chains on the mica surface. The desorption force was found to be increasing with increasing CaSO_4 concentration (cf. Fig. 16). The interpretation of these results still requires further investigation but they correspond to the known effect of polyanion binding induced by multivalent cations.

The experimental approach introduced for these types of desorption experiment can also be utilized to discriminate between Coulombic and non-Coulombic interactions as is indicated by Eq. (7). While it is straightforward to identify and characterize Coulombic contributions by investigating the relationship between the mean desorption force and the Debye screening length that is determined by the salt concentration in solution, the investigation of the constant term in Eq. (7) is much more difficult. This is due to the fact that the non-Coulombic offset F_0 generally consists of different contributions, e.g., van der Waals interactions or hydrogen bonds, that are hard to separate from each other. Nevertheless some of them can be identified by the analysis of differences in the adsorption characteristics induced by certain environmental changes. One example for such systematic investigations is desorption measurements performed with polyacrylic acid on self-assembled monolayers (SAMs).¹⁷⁴ The SAMs consisted of CH_3 -terminated, OH-terminated, and COOH-terminated alkylchains that represent a hydrophobic, a polar, and an acidic surface, respectively. The measurements were done with one and the same AFM tip, so that the results

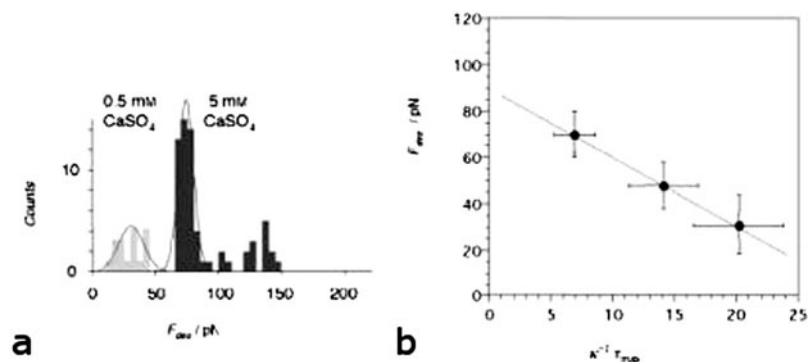


FIG. 16. (a) Desorption force histograms for polyacrylic acid on mica for different concentrations of CaSO_4 . The desorption force as well as the number of desorption events is strongly increasing when the CaSO_4 concentration is raised from 0.5 to 5 mM (b) Desorption force depicted against $\kappa^{-1}\tau_{\text{max}}$: The desorption force is increasing linearly when the CaSO_4 concentration is raised revealing an attractive ion-bridging interaction.

can be directly compared. In the desorption experiments the NaCl concentration was varied at a fixed pH of 6. The different surfaces displayed several characteristic features: only short plateaus were found on the CH_3 -SAM, longer ones on the OH-SAM, and the longest ones on the COOH-SAM. Additional facts can be extracted by having a closer look at the desorption force histograms: Three of them, representative for the measurements on the CH_3 -, the OH-, and the COOH-SAM, are shown in Fig. 17. For the CH_3 -SAM only one peak appears corresponding to the desorption of a single polyelectrolyte chain from the SAM surface, whereas for the OH-SAM a second peak and for the COOH-SAM at least a third peak can be identified, which represent the desorption of two and three polyelectrolyte strands in parallel, respectively. The number of desorption events found in a set of 500

force-extension curves was rather small for the CH_3 -SAM (30%), larger for the OH-SAM (100%), and largest for the COOH-SAM (200%, which means that on average two desorption events were found per force curve). This holds for the total number of desorption events as well as for single and multiple peaks in the force histograms as can be seen from Fig. 17. The mean desorption forces found for the three different SAM substrates are extracted from the histograms by a Gaussian fit of the first peak. In Fig. 18 they are plotted against the Debye screening length. A linear dependency of the desorption force on the salt concentration could only be found in the case of CH_3 -SAM: the desorption force is found to be decreasing with the Debye screening length which indicates a repulsive electrostatic contribution that arises from a negative surface charge of the CH_3 -SAM. This

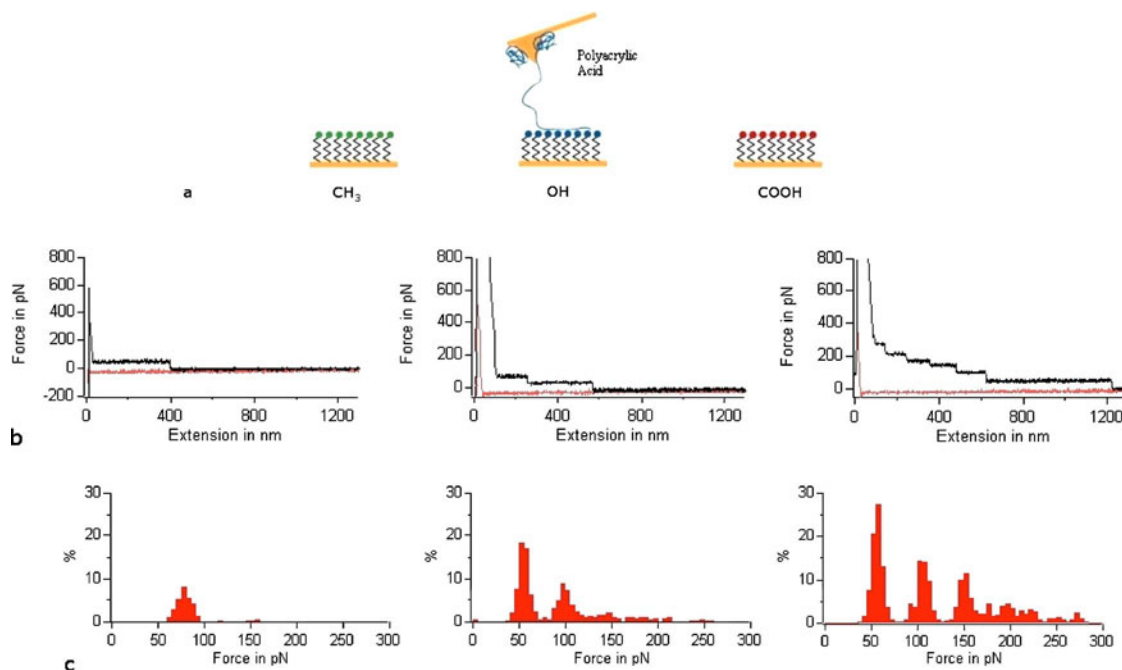


FIG. 17. (a) Desorption measurements of polyacrylic acid were performed with three different SAM surfaces: one is CH_3 -, the second is OH-, and the third one is COOH- terminated. All experiments took place in liquid environment with NaCl in solution. (b) Typical force-distance curves for the three substrates (5 mM NaCl, pH 6). When the cantilever is retracted in all three cases typical desorption plateaus were recorded (red: approach curve, black: retraction curve). If more than one step is observed multiple molecules with different lengths adsorbed onto the opposing SAM surfaces which were then desorbed upon retracting one after the other. (c) Histograms for the desorption forces (height of the desorption plateaus found in the force-extension curves) of polyacrylic acid measured for the three substrates. The first peak in the histograms corresponds to the desorption of single molecules, the following peaks to the desorption of two or more molecules. Each of the histograms was extracted from a set of 500 force-extension curves that were recorded with different NaCl concentrations. The histograms were normalized to the number of measured force curves.

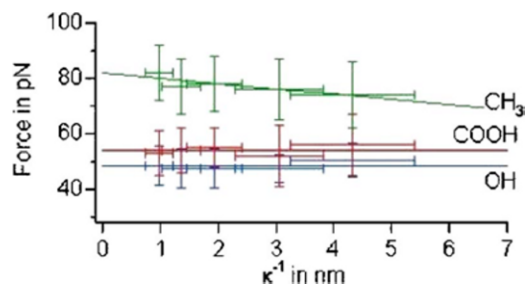


FIG. 18. Mean desorption force depicted against Debye screening length. The non-Coulombic contribution to the desorption force for the OH-SAM (48 pN) is the lowest. The non-Coulombic contribution for the COOH-SAM is slightly higher (54 pN) while the one for the CH₃-SAM is remarkably higher (77 pN). In the case of the CH₃-SAM a repulsive electrostatic interaction can be identified.

is well in agreement with measurements performed by Schweiss *et al.*¹⁷⁵ who determined the surface potential of a CH₃-terminated SAM to be -70 mV by zeta-potential measurements. The negative potential is attributed to adsorbed hydroxid ions at the SAM surface. Surprisingly for the OH- and the COOH-SAM no significant dependence on the Debye screening length was found. This means that the adsorption is dominated by non-Coulombic interactions for these surfaces. The desorption forces for the COOH- and the OH-SAM lie in the same range for both ions (50 pN), whereas the desorption force is significantly higher on the CH₃-SAM (80 pN). These results can be explained in a consistent form if energetical barriers are assumed for the CH₃-SAM which could be due to the water structure close to the SAM surface.¹⁷⁴

Additional measurements performed with the positively charged polyallylamine (PAL) confirmed the surprising fact that the hydrophobic CH₃ shows an effective negative charge which is almost half as large as a strongly charged surface. The comparison of the results for PAL with those obtained for PAA showed the same asymmetric behavior that could already be observed in the measurements done on calcite. A recent work investigated this feature in more detail.¹⁷⁶ That analysis indicates that Eq. (7) represents an oversimplification and additional facts have to be taken into account. Most importantly, the charge of most PEs is determined by a chemical equilibrium between charged and uncharged versions of their monomers. Due to electrostatic repulsion between charges on neighboring monomers, the degree of dissociation α of a PE differs significantly from single monomers, giving rise to a dramatically reduced line charge density at typical pH values.¹⁷⁷⁻¹⁸⁰ Upon adsorption, the dissociation equilibrium shifts,¹⁸¹ which in turn influences the adsorption energy and should be taken into account as well when modeling PE adsorption.

Salt-dependent adsorption energies of single anionic polyacrylic acid and cationic polyallylamine molecules on three different substrates, namely on a hydrophobic methyl-terminated self-assembled monolayer, on a strongly cationic ammonium-silanized silicon surface, and on metallic substrates were investigated. The latter ones showed larger non-

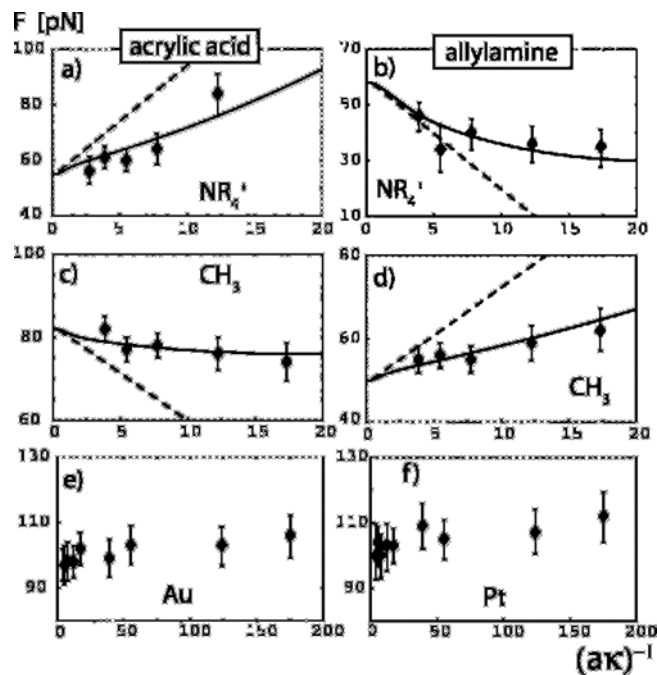


FIG. 19. Plateau desorption forces as a function of the rescaled Debye length $(\kappa a)^{-1}$ for: (a) polyacrylic acid (PAA) and (b) polyallylamine (PAL) on ammonium-silanized silicon, fitted by a surface charge of $\sigma = 0.11 \text{ nm}^{-2}$ with and without charge regulation on the polymers (solid and broken lines); (c) PAA; and (d) PAL on hydrophobic CH₃-terminated substrates, fitted by $\sigma = -0.064 \text{ nm}^{-2}$ (solid and broken lines); (e) PAA on gold and (f) PAL on platinum. The data in (a)–(d) are obtained with NaCl solutions at pH=6, and (e)–(f) with NaF solutions at fixed pH=7.

electrostatic binding than hydrophobic substrates, which is surprising since the PE backbones are mildly hydrophobic. Both PEs are vinyl based and have the same nominal charge density (corresponding to a charge separation of $a = 0.25$ nm), but the magnitude of the electrostatic adsorption energy on the cationic substrate is very different for the cationic and anionic PEs. Quantitative modeling of the adsorption energy was found to be only possible if one takes the salt and surface-charge dependent charge regulation of the polymers into account.

In Fig. 19 mean plateau forces for anionic (a), (c), (e) and cationic (b), (d), (f) PEs were plotted versus the rescaled screening length $(\kappa a)^{-1}$. In (a)–(b) results for an ammonium-silanized silicon surface are shown, whose large positive surface charge is due to quarternary amines and is thus pH independent. The nonelectrostatic adsorption energy [obtained in the limit $1/(\kappa a) = 0$] is on the order of $aF_0 \approx 4k_B T$ per monomer. The anionic PE is electrostatically attracted to the substrate, while the cationic PE is repelled, as expected. However, the slopes of the adsorption energies are very different, which will be interpreted in terms of surface-induced PE charge regulation. The salt dependence for the hydrophobic CH₃-terminated SAM [Figs. 19(c) and 19(d)] can be rationalized by a negative substrate charge. This is in qualitative agreement with ζ potential measurements¹⁷⁵ and has been associated with adsorption of OH⁻ ions on alkane monolayers¹⁸² as already mentioned above. The results in

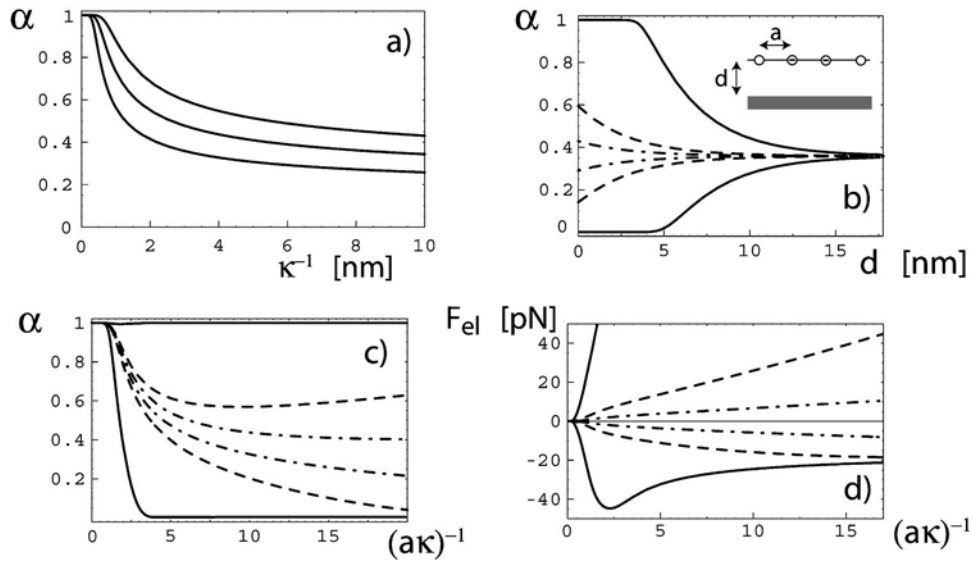


FIG. 20. (a) Mean-field results for the dissociation fraction α of a poly-anion in the bulk with monomer separation $a=0.25$ nm for fixed $pH-pK_s=2,3,4$ (from bottom to top) as a function of the screening length κ^{-1} . (b) α for fixed $pH-pK_s=2$ and $\kappa^{-1}=3$ nm as a function of the distance d to a charged surface with charge number density $\sigma=+0.048, -0.048$ nm $^{-2}$ (upper and lower dashed-dotted line, respectively) and $\sigma=\pm 0.16, \pm 1.6$ nm $^{-2}$ (dashed and solid lines). (c) α for fixed $pH-pK_s=2$, $d=a=0.25$ nm (mimicking a surface-adsorbed polyanion) and the same surface charge densities as in (b). (d) Electrostatic desorption forces F_{el} for the same parameters as in (c).

Figs. 19(e) and 19(f) for polyallylamine on gold and platinum are obtained with NaF since fluorides show a low affinity to metal surfaces. The adsorption behavior of PEs on metals has been predicted to be dominated by image-charge attraction, leading to a logarithmic (and thus very weak) dependence on the screening length,¹⁸³ in qualitative accord with the experimental results in Figs. 19(e) and 19(f). No quantitative comparison of the data with theoretical predictions is attempted, though, since the electrostatic contribution is on the order of the experimental errorbars. Surprisingly, the nonelectrostatic component on metals is the strongest of all substrates examined.

To simplify the theoretical modeling of surface-induced PE charge regulation the PE was regarded as a straight rod with dissociable charges separated by the distance a . The thermodynamic average over the microscopic energy expression $H/k_B T = \mu \sum_i s_i + \sum_{i>j} s_i s_j v_{DH}[a(i-j)]$, where s_i denotes the fluctuating state variable of monomer site i which is 1 when the site is charged and 0 when it is neutral, delivers the mean fraction of dissociated sites α . The electrostatic interaction can be approximated by the use of a Debye-Hückel (DH) potential $v_{DH}(r) = l_B e^{-r/\kappa} / r$. The chemical potential was $\mu = -2.303(pH - pK_s) - l_B \kappa + \psi / k_B T$. This includes the electrostatic potential due to a charged surface at separation d which reads on the linear level $\psi / k_B T = 4\pi l_B \sigma \kappa^{-1} e^{-d\kappa}$. All monomers were assumed to have the same distance from the surface [see inset Fig. 20(b)]. In the presence of long-ranged charge repulsions, nearest-neighbor approximations are no longer valid,¹⁷⁹ while exact calculation of the mean charge fraction $\alpha = \langle s_i \rangle$ is tedious. The problem can be solved by the use of mean-field theory which provides a simple yet accurate close-form solution¹⁸⁰

$$2.303(pH - pK_s) = \ln \frac{\alpha}{1 - \alpha} + \Delta \alpha - l_B \kappa + 4\pi l_B \sigma \kappa^{-1} e^{-\kappa d}, \quad (8)$$

which can numerically or graphically be inverted. In this case, $\Delta = -2(l_B/a) \ln(1 - e^{-\kappa a})$ is the coupling parameter which takes charge-repulsion between neighboring monomers into account. If $\Delta = 0$ (obtained for large salt concentration $\kappa a \gg 1$) the usual “law-of-mass-action” dissociation behavior is obtained, where as for $\Delta \neq 0$ the dissociation is greatly reduced. Figure 20(a) shows α for a polyacid with monomer separation $a=0.25$ nm for fixed $pH-pK_s=2,3,4$ (from bottom to top) as function of the screening length in the bulk, i.e., in the absence of a charged surface. It is a well known fact that the dissociation for all but very high salt concentrations (small κ^{-1}) is incomplete and further decreases with increasing κ^{-1} . This phenomenon is known as charge regulation. Figure 20(b) shows α for fixed $pH-pK_s=2$ and $\kappa^{-1}=3$ nm for a few different surface charge densities as a function of the distance d from the surface. As can be clearly seen charge regulation is dramatically changed at a charged surface. In brief, the polyanion charge increases at a cationic surface (upper curves) and decreases at an anionic surface (lower curves) for distances smaller than the screening length κ^{-1} . Figure 20(c) shows the dissociation rate at constant pH , for various surface charge densities at a fixed distance $d=a=0.25$ nm from the surface, which can be correlated with the state of an adsorbed PE, as a function of the rescaled screening length (note that the resulting behavior depends only very weakly on the precise value of the surface distance in the adsorbed state). In this case the behavior is

quite complex: It results from the conflicting tendencies of high salt to increase the dissociation [cf. Fig. 20(a) for the bulk case] but also to screen the surface-polymer interaction, which leads to an increase in α for large κ^{-1} in the case of a cationic substrate (see for example upper broken line). The electrostatic contribution to the plateau desorption force, F_{el} , is determined as the free energy difference of the charged polymer in the adsorbed surface state and in bulk, $F_{el} = -[\mathcal{F}(z=d) - \mathcal{F}(z=\infty)]/a$. The free energy per monomer is then given by $\mathcal{F}/k_B T = \alpha \ln \alpha + (1-\alpha) \ln(1-\alpha) + \Delta \alpha^2/2 + \mu \alpha$ within mean-field theory. The plateau force is shown in Fig. 20(d) for the same parameters as in Fig. 20(c). The main result is that the response of a PE to cationic and anionic surfaces is quite asymmetric: If the surface is attractive the PE becomes fully charged ($\alpha=1$) at high and low salt concentrations [upper curves in Fig. 20(c)], and the adsorption energy becomes proportional to the surface potential ψ and thus to κ^{-1} . On the other hand, if the interactions between PE and surface are repulsive (i.e., a polyacid on an anionic substrate), the effective charge goes down at low salt concentration and the electrostatic contribution to the plateau force goes to zero as $\kappa^{-1} a \gg 1$.

The solid lines in Figs. 19(a)–19(e) show the theoretically predicted plateau force F_{el} using the surface-dependent charge regulated α as given by Eq. (8) as solid lines, where the surface charge of ammonium-silanized silicon was adjusted as $\sigma=0.11 \text{ nm}^{-2}$ and of the hydrophobic methyl-terminated self-assembled monolayer as $\sigma=-0.064 \text{ nm}^{-2}$. For the monomeric dissociation constant of polyacrylic acid (PAA) we used $pK_s=4.6$, while for polyallylamine (PAL) we used $pK_b=10.6$. Most importantly, the experimental data for cationic and anionic PE can simultaneously be described with one surface charge density, and leads to a quite robust fit of the nonelectrostatic binding energy [which is the asymptote as $1/(a\kappa) \rightarrow 0$]. Although the experimental pH was chosen such that PAL (with $pK_b - pH=4.6$) in bulk has a higher charge than PAA (with $pH - pK_s=1.4$), the reduction of the plateau force for PAL in Fig. 19(b) is smaller than the enhancement for PAA in Fig. 19(a) for large screening lengths. This can only be understood in terms of surface-induced PE charge regulation. This is brought out clearly by the broken lines, which are the plateau forces $F_{el} = \psi/a$ for full charging $\alpha=1$ with the same surface charge density values σ as for the solid lines. (Note that no regulation has to be taken into account for the substrate, since it is caused by a quarternary ammonium.) The surface charge density of the ammonium silanized surface has been estimated to be below $\sigma=0.2^{-2}$.¹⁸⁴ This corresponds well to the result of our investigations which give a charge of $\sigma=0.11^{-2}$. The fits for the hydrophobic methyl-terminated SAMs give a negative charge of $\sigma=-0.064 \text{ nm}^{-2}$, which is comparable to the value $\sigma=-0.028 \text{ nm}^{-2}$ that can be derived from zeta-potential measurements¹⁷⁵ (using the zeta potential $\psi=-0.35 \text{ mV}$ for a salt concentration $c_s=3 \text{ mM}$, $pH=6$, and the DH conversion $\psi/k_B T = 4\pi l_B \sigma / \kappa$). The agreement is satisfactory given that two very disparate techniques are compared (remembering that the zeta potential is defined at the plane of shear which

does not necessarily coincide with the adsorption height of polymers), and shows that the negative zeta potential is not a kinetic artifact but has a real counterpart in terms of an interaction free energy.

In all investigations presented so far the plateau force contribution F_{en} due to the conformational entropy difference between the planar compressed adsorbed PE section and the stretched desorbed PE section was neglected. This contribution has also been estimated recently. The compression magnitude in the adsorbed state is unknown. In the following we estimate the plateau-force contribution due to the stretching of the desorbed section: For a Gaussian chain of polymerization index N and Kuhn length b (which should not be confused with the bond length a) the free energy \mathcal{F} is increasing with the stretching force F as $\mathcal{F} = F^2 b^2 N / (6k_B T)$, which is valid until a critical force $F^* = 3k_B T / b$ at which the chain is completely stretched. Thus, the stretching contribution F_{str} to the total plateau force F is given by $F_{str} = \mathcal{F} / (aN) = F^2 b / (6k_B T)$. At the critical force $F = F^*$ this reduces to $F_{str} = 3k_B T / 2b$. For a Kuhn length $b \approx 1 \text{ nm}$ this thus results in $F_{str} \approx 6 \text{ pN}$, which is negligible (forces larger than the critical force give only additional logarithmic contributions).

V. STRETCHING OF SINGLE POLYMERS

In this section we describe a detailed joint experimental/theoretical study on the stretching behavior of different polymers which are irreversibly attached between substrate and AFM tip. As is well known, single polymers show a strongly nonlinear behavior when they are stretched by an external force. Different force regimes are distinguished: The low force regime is dominated by purely entropic contributions that result from the disentanglement of the Gaussian polymer coil. The high force regime is dominated by enthalpic contribution and in the medium range conformational changes of the polymer may occur.

Two simple models are commonly used for describing the entropic contribution: The freely jointed chain model (FJC)¹⁸⁵ and the worm-like chain model (WLC).^{186,187} In the FJC model a polymer is regarded as a chain with N inextensible segments of length l . The individual segments are freely jointed without spatial restrictions for their arrangement. Each segment can be oriented in every direction with equal probability. The contour length is given by $L = N \cdot l$. The mean extension R is derived from the chains partition function at constant force, Z_F

$$Z_F = \int_{l_1} \cdots \int_{l_N} \exp - \frac{F \cdot R}{k_B T} dl_1 \cdots dl_N, \quad (9)$$

where l_1, \dots, l_N are the bond vectors for the N segments. The mean extension along the z axis R is obtained as a function of the applied force as

$$R = N \cdot l \cdot \left[\coth \left(\frac{F \cdot l}{k_B T} - \frac{k_B T}{F \cdot l} \right) \right] = N \cdot l \cdot \mathbf{L} \left(\frac{F \cdot l}{k_B T} \right), \quad (10)$$

where $\mathbf{L}(x) := \coth(x) - x^{-1}$ is the Langevin function. The average force in the z direction is obtained by the inversion of

this relation. The segment length l , which is a measure for the flexibility of the random coil, is the only relevant fit parameter in this model. It can be identical to the length of a monomer unit, but in most cases the values for flexible polymers in good solvent conditions differ from this value.

The WLC model entirely neglects any discrete structure along the chain. The polymer is described as a continuous string $\mathbf{r}(s)$ of constant bending modulus B . The flexibility of the polymer coil is determined by the elastic bending energy E_B that is given by

$$E_B = \frac{B}{2} \cdot \int \left(\frac{\partial^2 \mathbf{r}}{\partial s^2} \right)^2 ds \quad (11)$$

The characteristic length scale that is a measure for the flexibility of the polymer in this model is represented by the persistence length L_p . The persistence length is defined as the decay length of the directional correlation along the polymer chain and is therefore given by $L_p = B/(k_B T)$. An exact force-distance relation of a WLC can only be determined numerically, but a commonly used analytical approximation is given by:¹⁸⁸

$$F = \frac{k_B T}{L_p} \cdot \left[\frac{R}{L} - \frac{F}{K_0} + \frac{1}{4 \left(1 - \frac{R}{L} + \frac{F}{K_0} \right)^2} - \frac{1}{4} \right]. \quad (12)$$

This approximation is exact for $R \rightarrow 0$ and $R \rightarrow L$ but in the intermediate regime deviations up to 10% for $R/L \approx 0.5$ occur which may result in an overestimation of L_p by approximately 5%.

So far only the entropic contribution is considered in these models which implies a fixed contour length L for the polymer backbone. This does not hold in the high force regime that exceeds the limit at which the covalent bonds of the chain break. Before the bonds finally break, the segment length will increase due to bond angle deformation and the stretching of the covalent bonds. Consequently, enthalpic contributions to the restoring force of the polymer chain must be taken into account. In the simplest approach the enthalpic contribution is just added as an additional Hookean term F_E , which scales linearly with the relative extension and is given by

$$F_E = K_0 \cdot \left(\frac{R}{N \cdot l} \right), \quad (13)$$

where K_0 means the (normalized) segment elasticity, which is a measure for the extensibility of the polymer chain. K_0 is introduced as an additional parameter into the polymer fit.

Another feature that has to be considered is the fact that polymers often undergo conformational or configurational transitions upon stretching. Usually such a change is marked by a striking deviation from the simple FJC or WLC form, e.g., a transition plateau if the transition is accompanied by a remarkable change in length. Examples for this are polysaccharides,⁷⁴ poly(ethylene glycol),¹⁸⁹ or DNA.¹⁰⁸ In the case of polysaccharides these transitional changes were attributed to conformational transitions in the pyran ring un-

der high stretching forces. One remarkable finding in the case of poly(ethylene glycol) and poly(vinyl alcohol) was the fact that the transitions were not found in apolar media. For poly(ethylene glycol) this was attributed to a breakdown of the hydrogen-bonded solvation superstructure in water upon overstretching the helically folded equilibrium conformation of the polymer. This example shows how environmental parameters may impact the stretching behavior of single polymer chains. A more complex system is double stranded DNA that shows a couple of particular stretching features. One of them is a highly cooperative conformational transition from its natural form (B-DNA) to an overstretched and underwound conformation (S-DNA). Upon this transition the length of the molecule approximately doubles. A variety of theoretical models and molecular dynamics simulations dealt with this overstretching transition and in the meantime a detailed picture of the mechanical properties of DNA has been revealed, which explains the coupling of stretch and twist, of overstretching mechanics, and of base pairing forces.

The WLC model as well as the FJC model (both augmented by a linear stretching term) contain the polymer length, the persistence length, and the Hookean spring constant as fit parameters.^{188,190,191} Unfortunately, it has been found that even with these three parameters, the force-extension traces cannot be described in the full range of forces, i.e., the fit parameters depend considerably on the range of forces used for the fit.^{28,192} Thus it can be questioned whether the spring constant determined in such studies is in fact a material constant or if it rather functions as a heuristic parameter and makes up for imperfections of the fitting model employed. This is backed up by recent theoretical investigations showing that a freely-rotating chain (FRC) model (which is quite realistic for many synthetic and single-stranded biological polymers) shows a crossover from WLC behavior at small stretching forces to a discrete regime (which accounts for the discrete nature of the chain) at large forces.^{193,194} For polymers with a bond length of $b = 0.15$ nm this crossover occurs at a force of roughly 40 pN. Thus the WLC chain behavior is preempted for most forces probed with the AFM.

The FJC or WLC have been applied to describe the behavior of polymers, when their conformational entropy is probed in the low force range,¹⁸⁸ while energetic contributions due to stretching of the polymer backbone have been described by *ab initio* calculations at higher forces up to 300 pN.¹⁹⁵ Using quantum-chemical *ab initio* methods, the elastic properties of polymeric bulk substances^{196,197} and the stretching behavior of single polyethylene-glycol molecules^{195,198} have been successfully predicted and compared with experiments. In a recent article that concentrates on the large force regime above 500 pN, where conformational polymer fluctuations constitute only small corrections to the stretching response, it was shown that in the high force regime quantitative agreement between experimental stretching curves and *ab initio* quantum-chemistry calculations is obtained with the contour length of the polymers as the only fitting parameter. The entropic force contribution

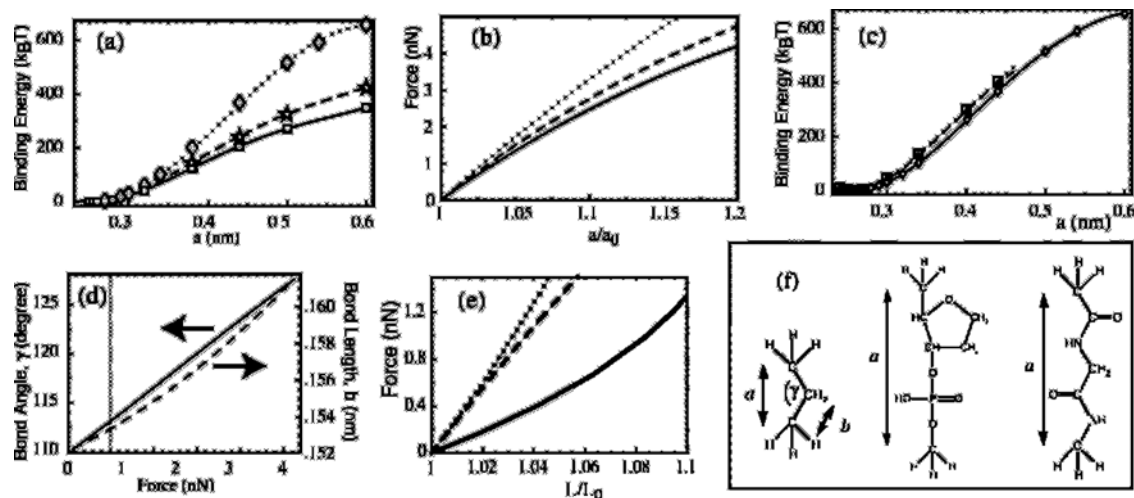


FIG. 21. (a) Total binding energy (relative to the ground state) and (b) stretching force for a propane molecule using three different quantum-chemical schemes, namely STO-6G (diamonds), TZV (stars) and TZV-MP2 (squares). The lines denote polynomial fits. (c) Binding energies per unit cell for an alkane chain consisting of three, seven, and 11 carbon atoms (diamonds, triangles, squares, respectively), showing the irrelevance of finite-size effects. (d) Bond angle (solid line) and bond length (broken line) as a function of the force for a propane molecule. (e) *Ab initio* (TZV-MP2) force-extension relation for ss-DNA, propane, and peptide (solid, broken, dotted line, respectively). (f) Structural formulas used in the calculations for propane, DNA, and a di-peptide unit.

due to chain conformational fluctuations can for large forces (within the discrete-chain regime) be accounted for without additional fitting parameters.¹⁹⁹

In *ab initio* methods one obtains the ground-state energy of a certain molecular configuration on the basis of the Schrödinger equation, within various numerical approximation schemes. As an illustration, in Fig. 21(a) the total binding energy (relative to the ground state) as a function of the unit-cell length a for a propane molecule [structure shown in Fig. 21(f)], which forms the smallest geometric subunit of an alkane chain, is presented. In the calculations only the distance of the two outer carbon atoms a was fixed, while the positions of all other nuclei were optimized such as to minimize the overall energy. The results were compared for three different levels of quantum-chemical calculations,²⁰⁰ namely Hartree-Fock (HF) with a rather small basis set consisting of six Gaussian-Slater-type orbitals (STO-6G, diamonds), HF with the more refined triple-zeta-valence basis set (TZV) (stars), and Moller-Plesset-2 which takes electron correlations into account (TZV-MP2) (squares). The latter, most advanced calculation, was used for the comparison with experiments. The difference between the various schemes illustrates the systematic errors involved in such *ab initio* calculations. The lines in Fig. 21(a) denote polynomial fits. What is really measurable experimentally is the force, which follows from the calculated energy curves by a derivative. The complete force functions are plotted in Fig. 21(b) and demonstrate that higher-order, nonlinear terms are important in the force range considered in AFM experiments. Figure 21(c) compares binding energies for alkane chains consisting of 3, 7, and 11 carbon atoms (diamonds, triangles, squares, respectively), all performed with the restrictive basis set STO-6G. The good agreement shows that finite-size effects are less important than the quality of basis sets used in the *ab initio* calculations. The influence of side chains (in spe-

cific amine, hydroxyl, and carboxyl groups) or solvent properties (by modeling water as a uniform polarizable continuum medium with relative dielectric constant $\epsilon=78$) on the elastic properties were also checked and it was found that there was no effect on forces larger than about 50 pN. Figure 21(d) shows the propane bond angle γ (solid line) and the bond length b [broken line, both are defined in Fig. 21(f)] as a function of the applied force. Both quantities change simultaneously with the applied force. The customary distinction between a hard degree of freedom (usually the bond length) and a soft degree of freedom (typically the bond angle) is incorrect; the elastic response of a chain involves changes of both.

These *ab initio* calculations were applied to three different experimentally investigated polymer architectures, namely ss-DNA, polyvinylamine, and peptide molecules (comparing poly-lysine, polyGVGVP, and titin) at stretching forces up to 2 nN. This was made possible by very stable attachments between polymers and cantilever tips and substrate surfaces, as described in the previous sections. Figure 21(e) presents the main theoretical result, the force versus relative elongation L/L_0 for the different polymer structures considered experimentally, namely alkane, ss-DNA, and peptide backbones (broken, solid, dotted line, all on the HF-TZV-MP2 level). By definition, all curves cross for zero elongation $L/L_0=1$. Figure 21(f) shows the corresponding chemical structures and unit cells used in the calculations. In all calculations, side chains have been stripped off, as they have been shown not to influence the results and the minimal unit cell which can be periodically repeated to build a long polymer is considered. In comparing experimental stretching curves with the *ab initio* prediction in Fig. 21(e) the contour length L_0 of the polymer is the only adjustable parameter, which is obtained with high precision. The spring constants of the polymers should not greatly exceed the probe spring

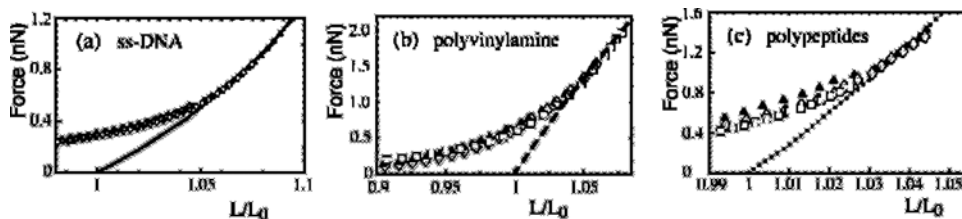


FIG. 22. Comparison of the *ab initio* predictions from Fig. 21(e) with each of three experimental curves for: (a) ss-DNA, (b) polyvinylamine, (c) peptide chains, namely polyGVGVP (open diamonds), titin (filled triangles), and poly-lysine (open squares). All experimental data were normalized by the polymer's contour length at zero force L_0 .

constant. Force curves of short polymer strands were therefore not included in our comparison. In practice, one plots the experimental force versus distance data as a function of the rescaled extension L/L_0 and adjusts the parameter L_0 until the experimental data match the *ab initio* curve at large forces. Figure 22(a) shows the result of this fitting procedure with the data for ss-DNA. The resulting contour lengths are $L_0=438$, 3318, and 4017 nm (open stars, filled triangles, open diamonds, respectively). In Fig. 22(b) we show data for polyvinylamine (PVA) polymers with a hydrolysis fraction of 0.1 (filled triangle) and 0.5 (diamonds, square). The molecules were covalently attached to an epoxy-silanized Si_3N_4 AFM tip and an epoxy-silanized glass slide. The measurements were performed under different electrolyte concentrations: 5 mM NaCl, 40 mM NaCl, and 20 mM NaCl (triangles, diamonds, squares, respectively).²⁸ Contour lengths of $L_0=2697$, 311.5, and 4932 nm (diamonds, triangles, squares, respectively) were obtained. In Fig. 22(c) three different peptide polymers are shown, poly-peptide C-(GVGVP)_{n_x251}-C (provided by Dan Urry and attached to gold-coated glass slides and Olympus Biolever AFM tips in Millipore water¹⁹²) with a fitted contour length $L_0=263.6$ nm (open diamonds), titin (provided by Mathias Gautel and adsorbed on a gold-coated surface and picked up with an untreated unsharpened Si_3N_4 AFM tip in PBS buffer with $L_0=129.5$ nm (filled triangles), and poly-L-lysine (Sigma, 300 kD, adsorbed on a gold-coated surface and picked up with an untreated unsharpened Si_3N_4 AFM tip in PBS with additional 500 mM NaCl) with a contour length $L_0=638.6$ nm (open squares). All data in Figs. 22(a)–22(c) nicely collapse and agree with the corresponding *ab initio* curves for larger forces. For the different peptide chains this indicates that they are described by their backbone stretching behavior only. In conclusion, for forces above 0.5–1.0 nN (depending on the polymer type) the stretching behavior of a wide class of backbone architectures can be accurately modeled by zero-temperature quantum-chemistry calculations without any model assumptions, with the only fitting parameter being the polymer contour length.

At small forces considerable deviations between the *ab initio* curves and experimental data (cf. Fig. 22) are found which are presumably caused by the fact that polymer fluctuations have not been taken into account so far. The internal dynamics may make a significant contribution to the entropic elasticity and as a result the analysis of stiff but internally highly dynamic polymer chains with static models, e.g., the

WLC and the FJC, will result in low persistence lengths despite their high bending rigidities. In the context of the *ab initio* calculations that focus on the high force regime two questions are important in this context: How robust is our data analysis with respect to the presence of such thermal effects, and, specifically, how will the fitted contour length shift as a result? Recently, the stretching response of the so-called FRC model (which is quite accurate for alkane chains) was considered theoretically.¹⁹³ The most important finding was that at forces larger than the threshold $F^* = L_p k_B T / b^2$ (where L_p is the effective persistence length), in the discrete regime, the stretching behavior is that of a FJC model but with an effective bond length which is twice the true bond length b . The polymer extension, R_z can for $F > F^*$ approximately be written as

$$R_z = L[F][1 - k_B T / (2bF)], \quad (14)$$

where $L[F]$ is the force-dependent contour length. For smaller forces, semiflexible behavior is found. Since for an alkane chain $F^* \approx 40$ pN, the discrete regime is realized for all stretching data compared to the *ab initio* calculations in this article. The force-dependent contour length $L=L[F]$ is obtained from the *ab initio* data via inversion. In writing Eq. (14) the fact that the force-induced bond length and angle increase is quite small is used. In Fig. 23 the PVA data [already shown in Fig. 22(b)] are compared to the discrete-chain prediction Eq. (14) (solid line), taking into account the energetic contribution from the *ab initio* calculation (via $L[F]$) and the entropic chain-fluctuation contribution. No additional parameter enters, since the known bond length $b = 0.154$ nm is used. The agreement of the solid line with the

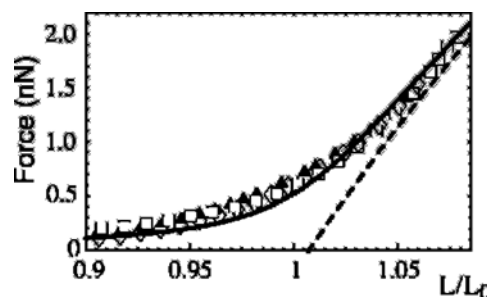


FIG. 23. PVA stretching data compared with the discrete chain prediction Eq. (14) including the *ab initio* contour length variation (solid line). The broken line denotes the zero-temperature limit without conformational fluctuations.

experimental data is remarkable, keeping in mind that no fitting parameter is used other than the chain contour length L_0 . By including the effects of fluctuations, the fitted contour lengths increase by a factor of 1.007, as is visualized by the broken line which follows from Eq. (14) by setting $k_B T = 0$ and thus corresponds to the zero-temperature limit. Fitting with the *ab initio* curves alone (without fluctuation corrections) thus gives reliable estimates of the chain lengths already, which is relevant for the more complicated peptide and ss-DNA molecules, where no effective model in terms of a simple FRC model is available.

VI. SUMMARY AND OUTLOOK

AFM-based force spectroscopy has in the last years evolved into a tool to study polymer elasticity and the energetics and kinetic of surface-polymer coupling at the single-molecule level. As such, many of the previously unknown microscopic parameters such as polymer stretching moduli and surface adsorption coefficients have been determined for various solution properties. Kinetic properties such as surface-friction coefficients are under scrutiny at present. The response of a surface-adsorbed polymer to a pulling force falls into one of two broad categories. If the polymer exhibits a negligible friction coefficient on the surface, it will glide over the surface when it is pulled by the AFM. In this case, the AFM can be utilized to study the desorption of single polyelectrolyte molecules from solid supports. Electrostatic interactions are characterized and separated from nonelectrostatic contributions. Single polyelectrolyte polymers can also be used as local probes to distinguish and characterize surfaces. Recent investigations that study the pulling-induced desorption of single polyelectrolytes from charged, hydrophobic, and metallic substrates revealed further surprising effects including surface induced charge regulation of the polyelectrolyte molecules and an enhanced desorption force found on metallic substrates which is attributed to image charge interactions.

For the case of polymers that are irreversibly fixed between surface and cantilever, AFM-based force spectroscopy in combination with theoretical methods has mapped out a more and more refined understanding of the stretching behavior of single polymer molecules. Rather simple polymer models like the FJC or the WLC models were found to be roughly capable of describing the observed stretching behavior. Quantum chemical *ab initio* calculations performed at zero temperature can be applied to describe the high force range of the polymer stretching curves. With the contour length L_0 as the only parameter, the agreement was found to be very good. Fluctuation effects could be reasonably described, without introducing additional free parameters, by incorporating recent results for the asymptotic large-force behavior of a FRC model. By using this approach it was found that at large forces of roughly 1 nN, the chemical structure changes substantially, i.e., bond angles and bond distances are perturbed quite considerably. This should help to develop mechanically controlled chemistry (certain reactions should be enhanced under mechanical stress) or to un-

derstand bond breakage under stress (which is important for controlling lubrication wear and failure). It was also shown that chemical single-polymer analysis could be feasible by comparison of experimental force traces and *ab initio* calculations at large forces, since different backbone architectures show quite different stretching responses. The results for the energetic and entropic polymer compliance can be useful in a variety of different polymer applications where large tensile forces act on polymers. Examples are strongly stretched polymer networks, where tensile stress is typically concentrated on a small fraction of all available chains and therefore locally very high, or dissolved polymers in high shear situations such as sheared polymer solutions at interfaces.

ACKNOWLEDGMENTS

This work was supported by the Deutsche Forschungsgemeinschaft (DFG) through SFB Grant Nos. 486 and SFB 563 and the Bayerische Elitekolleg Complex Interfaces.

- ¹U. Lemmer, *Polym. Adv. Technol.* **9**, 476 (1998).
- ²H. C. F. Martens, O. Hilt, H. B. Brom, P. W. M. Blom, and J. N. Huijberts, *Phys. Rev. Lett.* **87**, 086601 (2001).
- ³W. U. Huynh, J. J. Dittmer, and A. P. Alivisatos, *Science* **295**, 2425 (2002).
- ⁴F. Oosawa, *Polyelectrolytes* (Dekker, New York, 1971).
- ⁵J. Israelachvili, *Intermolecular and Surface Forces* (Academic, New York, 1992).
- ⁶H. Dautzenberg, W. Jaeger, B. P. J. Ktz, C. Seidel, and D. Stscherbind, *Polyelectrolytes: Formation, Characterization and Application* (Hanser, Munich, 1994).
- ⁷S. Förster and M. Schmidt, *Adv. Polym. Sci.* **120**, 51 (1995).
- ⁸G. J. Fleer, M. A. Cohen Stuart, J. M. H. M. Scheutjens, T. Gasgove, and B. Vincent, *Polymers at Interface* (Academic, London, 1995).
- ⁹R. R. Netz and D. Andelman, *Phys. Rep.* **380**, 1 (2003).
- ¹⁰P. H. Corkhill, A. S. Trevett, and B. J. Tighe, *Proc. Inst. Mech. Eng., Part A* **204**, 147 (1990).
- ¹¹T. T. Hesselink, *J. Colloid Interface Sci.* **60**, 448 (1977).
- ¹²G. J. Fleer and J. Lyklema, *J. Colloid Interface Sci.* **167**, 228 (1974).
- ¹³T. Matsumoto and Y. Adachi, *J. Colloid Interface Sci.* **204**, 328 (1998).
- ¹⁴D. Horn and F. Linkart, edited by Roberts (Blackie Academic & Professional, Glasgow, 1996).
- ¹⁵S. Mann, *Nature (London)* **332**, 119 (1988).
- ¹⁶S. Mann, J. Webb, R. J. P. Williams, *Biomaterialization: Chemical and Biochemical Perspectives* (VCH, Weinheim, 1989).
- ¹⁷L. Addadi and S. Weiner, *Angew. Chem.* **104**, 159 (1992).
- ¹⁸L. Qi, H. Cölfen, and M. Antonietti, *Angew. Chem.* **112**, 617 (2000).
- ¹⁹J. Y. Wong, J. Majewsky, M. Seitz, C. K. Park, J. N. Israelachvili, and G. S. Smith, *Biophys. J.* **77**, 1445 (1999).
- ²⁰J. Schmitt, T. Grünwald, K. Kjaer, P. Pershan, G. Decher, and M. Lösche, *Macromolecules* **26**, 7058 (1993).
- ²¹J. Rädler, I. Koltover, T. Salditt, and C. Safinya, *Science* **275**, 810 (1997).
- ²²P. G. Hartley and P. J. Scales, *Langmuir* **14**, 6948 (1998).
- ²³F. Caruso, D. N. Furlong, K. Ariga, I. Ichinose, and T. Kunitake, *Langmuir* **14**, 4559 (1998).
- ²⁴H. Clausen-Schauman and H. E. Gaub, *Langmuir* **15**, 8246 (1999).
- ²⁵Y. Kamiyama and J. Israelachvili, *Macromolecules* **25**, 5081 (1992).
- ²⁶M. A. G. Dahlgren and P. M. Claesson, *Prog. Colloid Polym. Sci.* **93**, 206 (1993).
- ²⁷X. Châtelier, T. J. Senden, and J. M. di Meglio, *Europhys. Lett.* **41**, 303 (1998).
- ²⁸T. Hugel, M. Grosholz, H. Clausen-Schaumann, A. Pfau, H. E. Gaub, and M. Seitz, *Macromolecules* **34**, 1039 (2001).
- ²⁹M. Seitz, C. Friedsam, W. Jöstl, T. Hugel, and H. E. Gaub, *ChemPhysChem* **4**, 986 (2003).
- ³⁰S. A. Sukhishvili, A. Dhinojwala, and S. Granick, *Langmuir* **15**, 8474 (1999).
- ³¹J. DeRouchey, R. R. Netz, and J. O. Raedler, *Eur. Phys. J. E* **16**, 17

- (2005).
- ³²B. J. Haupt, T. J. Senden, and E. M. Sevick, *Langmuir* **18**, 2174 (2002).
- ³³R. R. Netz and J.-F. Joanny, *Macromolecules* **32**, 9013 (1999).
- ³⁴J.-L. Barrat and J.-F. Joanny, *Adv. Chem. Phys.* **94**, 1 (1996).
- ³⁵C. Fleck, R. R. Netz, and H. H. von Grnberg, *Biophys. J.* **82**, 76 (2002).
- ³⁶A. Shafir, D. Andelman, and R. R. Netz, *J. Chem. Phys.* **119**, 2355 (2003).
- ³⁷R. R. Netz and D. Andelman, *Adsorbed and Grafted Polymers at Equilibrium* (Marcel Dekker, New York, 2000).
- ³⁸M. Muthukumar, *J. Chem. Phys.* **86**, 7230 (1987).
- ³⁹J.-F. Joanny, M. Castelnovo, and R. R. Netz, *J. Phys.: Condens. Matter* **12**, A1 (2000).
- ⁴⁰C. Y. Kong and M. Muthukumar, *J. Chem. Phys.* **109**, 1522 (1998).
- ⁴¹J.-L. Barrat and J.-F. Joanny, *Europhys. Lett.* **24**, 333 (1993).
- ⁴²A. V. Dobryin, A. Deshkovski, and M. Rubinstein, *Macromolecules* **34**, 3421 (2001).
- ⁴³C. Holm, J. F. Joanny, K. Kremer, R. R. Netz, P. Reineker, C. Seidel, T. A. Vilgis, and R. G. Winkler, *Adv. Polym. Sci.* **166**, 67 (2004).
- ⁴⁴H. Ahrens, S. Förster, C. A. Helm, N. A. Kumar, A. Naji, R. R. Netz, and C. Seidel, *J. Phys. Chem. B* **108**, 16870 (2004).
- ⁴⁵M. Manghi and R. R. Netz, *Eur. Phys. J. E* **14**, 67 (2004).
- ⁴⁶H. J. Kreuzer, *Chin. J. Phys. (Taipei)* **43**, 249 (2005).
- ⁴⁷*Handbook of Micro/Nano Tribology*, 1st Ed., edited by B. Bushan (CRC, Boca Raton, FL, 1995).
- ⁴⁸K. Kendall, *Science* **263**, 1720 (1994).
- ⁴⁹H. A. Rinia, J. W. Boots, R. A. Kik, M. M. E. Snel, R. A. Demel, J. A. Killian, J. P. van der Eerden, and B. de Kruijff, *Biochemistry* **41**, 2814 (2002).
- ⁵⁰H. A. Rinia, M. M. E. Snel, J. P. van der Eerden, and B. de Kruijff, *FEBS Lett.* **501**, 92 (2001).
- ⁵¹M. Seitz, C. K. Park, J. Y. Wong, and J. Israelachvili, *Langmuir* **17**, 4616 (2001).
- ⁵²S. Mann and H. E. Gaub, *Science* **270**, 1480 (1995).
- ⁵³C. Gliss, H. Clausen-Schaumann, R. Gnther, S. Odenbach, O. Randl, and T. M. Bayerl, *Biophys. J.* **74**, 2443 (1998).
- ⁵⁴F. Oesterhelt, D. Oesterhelt, M. Pfeiffer, A. Engel, H. E. Gaub, and D. J. Müller, *Science* **288**, 143 (2000).
- ⁵⁵D. J. Müller, M. Kessler, F. Oesterhelt, C. Müller, D. Oesterhelt, and H. E. Gaub, *Biophys. J.* **83**, 36321 (2002).
- ⁵⁶T. E. Fisher, S. F. Oberhauser, M. Carrion-Vazquez, P. E. Marszalek, and J. M. Fernandez, *Trends Biochem. Sci.* **24**, 379 (1999).
- ⁵⁷J. G. Duguid, V. A. Bloomfield, J. M. Benevides, and G. H. Thomas, Jr., *Biophys. J.* **71**, 3350 (1996).
- ⁵⁸S. Sharma, S. Bharadwaj, A. Suroliya, and S. K. Podder, *Biochem. J.* **333**, 539 (1998).
- ⁵⁹A. Homola and A. A. Robertson, *J. Colloid Interface Sci.* **312**, 286 (1976).
- ⁶⁰D. M. LeNeveau, R. P. Rand, and V. A. Parsegian, *Nature (London)* **259**, 601 (1976).
- ⁶¹D. Tabor and R. H. S. Winterton, *Proc. R. Soc. London, Ser. A* **312**, 435 (1969).
- ⁶²J. Israeachvili, *J. Colloid Interface Sci.* **44**, 259 (1973).
- ⁶³J. Israelachvili, *Acc. Chem. Res.* **20**, 415 (1987).
- ⁶⁴T. D. Stowe, K. Yasumura, T. W. Kenny, D. Botkin, K. Wago, and D. Rugar, *Appl. Phys. Lett.* **71**, 288 (1997).
- ⁶⁵A. Kishino and T. Yanagida, *Nature (London)* **334**, 74 (1988).
- ⁶⁶S. B. Smith, L. Finzi, and C. Bustamante, *Science* **258**, 1122 (1992).
- ⁶⁷J.-F. Allemand, These de doctorat, Ecole Normale Supérieure, France 1997.
- ⁶⁸T. R. Strick, J.-F. Allemand, D. Bensimon, and V. Croquette, *Science* **271**, 1835 (1996).
- ⁶⁹G. Binnig, C. F. Quate, and C. Gerber, *Phys. Rev. Lett.* **56**, 930 (1986).
- ⁷⁰G. Binnig and H. Rohrer, *Rev. Mod. Phys.* **59**, 615 (1987).
- ⁷¹F. Ohnesorge and G. Binnig, *Science* **260**, 1451 (1993).
- ⁷²K. D. Jandt, *Mater. Sci. Eng., R.* **21**, 221 (1998).
- ⁷³M. Radmacher, *IEEE Eng. Med. Biol. Mag.* **16**, 47 (1997).
- ⁷⁴M. Rief, F. Oesterhelt, B. Heymann, and H. E. Gaub, *Science* **275**, 1295 (1997).
- ⁷⁵E.-L. Florin, V. T. Moy, and H. E. Gaub, *Science* **264**, 415 (1994).
- ⁷⁶H. Heinzelmann, E. Meier, H. Rudin, and H. H. Güntherodt, *Force Microscopy in Scanning Tunneling Microscopy and Related Methods* (Kluwer-Academic, Amsterdam, 1990).
- ⁷⁷P. K. Hansma *et al.*, *Appl. Phys. Lett.* **64**, 1738 (1994).
- ⁷⁸H. G. Hansma and J. H. Hoh, *Annu. Rev. Biophys. Biomol. Struct.* **23**, 115 (1994).
- ⁷⁹M. B. Viani *et al.*, *Rev. Sci. Instrum.* **70**, 4300 (1999).
- ⁸⁰G. U. Lee, L. A. Chris, and R. J. Colton, *Science* **266**, 771 (1994).
- ⁸¹A. Noy, D. V. Vezenov, and C. M. Lieber, *Annu. Rev. Mater. Sci.* **27**, 381 (1997).
- ⁸²A. Ashkin, K. Schütze, J. M. Dziedzic, U. Euteneuer, and M. Schliwa, *Nature (London)* **348**, 346 (1990).
- ⁸³M. P. Sheetz, *Laser Tweezers in Cell Biology* (Academic, New York, 1997).
- ⁸⁴S. M. Block, *Nature (London)* **360**, 493 (1992).
- ⁸⁵S. Chu, *Sci. Am.* **71** (1992).
- ⁸⁶K. Svoboda and S. M. Block, *Annu. Rev. Biophys. Biomol. Struct.* **23**, 247 (1994).
- ⁸⁷R. Alon, D. A. Hammer, and T. A. Springer, *Nature (London)* **374**, 539 (1995).
- ⁸⁸G. Kaplanski, C. Farnarier, O. Tissot, A. Pierres, A.-M. Benoliel, M.-C. Alessi, S. Kaplanski, and P. Bongrand, *Biophys. J.* **64**, 1922 (1993).
- ⁸⁹D. Kwong, D. F. J. Tees, and H. L. Goldsmith, *Biophys. J.* **71**, 1115 (1996).
- ⁹⁰D. F. J. Tees, O. Coenen, and H. L. Goldsmith, *Biophys. J.* **65**, 1318 (1993).
- ⁹¹D. F. J. Tees and H. L. Goldsmith, *Biophys. J.* **71**, 1102 (1996).
- ⁹²S. P. Tha, J. Shuster, and H. L. Goldsmith, *Biophys. J.* **50**, 1117 (1986).
- ⁹³E. Evans, K. Ritchie, and R. Merkel, *Biophys. J.* **68**, 2580 (1995).
- ⁹⁴D. A. Simson, F. Ziemann, M. Strigl, and R. Merkel, *Biophys. J.* **74**, 2080 (1998).
- ⁹⁵N. H. Thomson, M. Fritz, M. Radmacher, C. F. Schmidt, and P. K. Hansma, *Biophys. J.* **70**, 2421 (1996).
- ⁹⁶T. Strunz, K. Oroszlan, R. Shafer, and H.-J. Güntherodt, *Proc. Natl. Acad. Sci. U.S.A.* **96**, 11277 (1999).
- ⁹⁷D. Krüger, H. Fuchs, R. Rousseau, D. Marx, and M. Parrinello, *Phys. Rev. Lett.* **89**, 186402 (2002).
- ⁹⁸J. F. Allemand, D. Bensimon, L. Jullien, A. Bensimon, and V. Croquette, *Biophys. J.* **73**, 2064 (1997).
- ⁹⁹A. D. Mehta, M. Rief, J. A. Spudich, D. A. Smith, and R. M. Simmons, *Science* **283**, 1689 (1999).
- ¹⁰⁰A. Janshoff, M. Neitzert, Y. Oberdörfer, and H. Fuchs, *Angew. Chem.* **112**, 3346 (2000).
- ¹⁰¹U. Dammer, M. Hegner, D. Anselmetti, P. Wagner, M. Dreier, W. Huber, and H.-J. Güntherodt, *Biophys. J.* **70**, 2437 (1996).
- ¹⁰²W. Dettmann, M. Grandbois, S. Andr, M. Benoit, A. K. Wehle, H. Kaltner, H.-J. Gabius, and H. E. Gaub, *Arch. Biochem. Biophys.* **383**, 157 (2000).
- ¹⁰³M. Grandbois, M. Beyer, M. Rief, H. Clausen-Schaumann, and H. E. Gaub, *Science* **283**, 1727 (1999).
- ¹⁰⁴W. F. Heinz and J. H. Hoh, *Trends Biotechnol.* **17**, 143 (1999).
- ¹⁰⁵A. Janshoff, M. Neitzert, Y. Oberdörfer, and H. Fuchs, *Angew. Chem., Int. Ed. Engl.* **112**, 3346 (2000).
- ¹⁰⁶H. Clausen-Schaumann, M. Seitz, R. Krautbauer, and H. Gaub, *Curr. Opin. Chem. Biol.* **4**, 524 (2000).
- ¹⁰⁷G. U. Lee, D. A. Kidwell, and R. J. Colton, *Langmuir* **10**, 354 (1994).
- ¹⁰⁸H. Clausen-Schaumann, M. Rief, C. Tolksdorf, and H. E. Gaub, *Biophys. J.* **78**, 1997 (2000).
- ¹⁰⁹P. E. Marszalek, A. F. Oberhauser, Y. P. Pang, and J. M. Fernandez, *Nature (London)* **396**, 661 (1998).
- ¹¹⁰M. Rief, M. Gautel, F. Oesterhelt, J. M. Fernandez, and H. E. Gaub, *Science* **276**, 1109 (1997).
- ¹¹¹M. S. Kellermayer, S. B. Smith, H. L. Granzier, and C. Bustamante, *Science* **276**, 1112 (1997).
- ¹¹²A. F. Oberhauser, P. E. Marszalek, H. P. Erickson, and J. M. Fernandez, *Nature (London)* **393**, 181 (1998).
- ¹¹³M. Rief, M. Gautel, A. Schemmel, and H. E. Gaub, *Biophys. J.* **75**, 3008 (1998).
- ¹¹⁴P. E. Marszalek, H. Lu, H. B. Li, M. Carrion-Vazquez, A. F. Oberhauser, K. Schulten, and J. M. Fernandez, *Nature (London)* **402**, 100 (1999).
- ¹¹⁵M. Carrion-Vazquez, A. F. Oberhauser, S. B. Fowler, P. E. Marszalek, S. E. Broedel, J. Clarke, and J. M. Fernandez, *Proc. Natl. Acad. Sci. U.S.A.* **96**, 3694 (1999).
- ¹¹⁶P. Cluzel, A. Lebrun, C. Heller, R. Lavery, J.-L. Viovy, D. Chatenay, and F. Caron, *Science* **271**, 792 (1996).
- ¹¹⁷H. Dietz and M. Rief, *Proc. Natl. Acad. Sci. U.S.A.* **101**, 16192 (2004).
- ¹¹⁸I. Schwaiger, A. Kardinal, M. Schleicher, A. A. Noegel, and M. Rief, *Nat.*

- Struct. Biol. **11**, 81 (2004).
- ¹¹⁹D. K. Klimov and D. Thirumalai, Proc. Natl. Acad. Sci. U.S.A. **96**, 6166 (1999).
- ¹²⁰M. Rief, J. Pascual, M. Saraste, and H. E. Gaub, J. Mol. Biol. **286**, 553 (1999).
- ¹²¹R. Krautbauer, H. Clausen-Schaumann, and H. E. Gaub, Angew. Chem., Int. Ed. Engl. **39**, 3912 (2000).
- ¹²²G. I. Bell, Science **200**, 618 (1978).
- ¹²³E. Evans, D. Berk, and A. Leung, Biophys. J. **59**, 838 (1991).
- ¹²⁴E. Evans and K. Ritchie, Biophys. J. **72**, 1541 (1997).
- ¹²⁵S. Israilev, S. Stepaniants, M. Balsera, Y. Ono, and K. Schulten, Biophys. J. **72**, 1568 (1997).
- ¹²⁶H. Grubmüller, B. Heymann, and P. Tavan, Science **271**, 997 (1996).
- ¹²⁷R. Merkel, P. Nassoy, A. Leung, K. Ritchie, and E. Evans, Nature (London) **397**, 50 (1999).
- ¹²⁸E. Evans and F. Ludwig, J. Phys.: Condens. Matter **12A**, 315 (2000).
- ¹²⁹E. Evans, Annu. Rev. Biophys. Biomol. Struct. **30**, 105 (2001).
- ¹³⁰E. Evans, Biophys. Chem. **82**, 83 (1999).
- ¹³¹E. Evans, Faraday Discuss. **111**, 1 (1998).
- ¹³²B. Heymann and H. Grubmüller, Phys. Rev. Lett. **84**, 6126 (2000).
- ¹³³B. Heymann and H. Grubmüller, Biophys. J. **81**, 1295 (2001).
- ¹³⁴B. Heymann and H. Grubmüller, Chem. Phys. Lett. **303**, 1 (1999).
- ¹³⁵M. Balsera, S. Stepaniants, S. Israilev, Y. Oono, and K. J. Schulten, Biophys. J. **73**, 1281 (1997).
- ¹³⁶S. Boresch and M. Karplus, J. Mol. Biol. **254**, 801 (1995).
- ¹³⁷J. Shillcock and U. Seifert, Phys. Rev. E **57**, 7301 (1998).
- ¹³⁸U. Seifert, Phys. Rev. Lett. **84**, 2750 (2000).
- ¹³⁹G. Hummer and A. Szabo, Proc. Natl. Acad. Sci. U.S.A. **98**, 3658 (2001).
- ¹⁴⁰X. Châtelier, T. J. Senden, and J. M. di Meglio, Europhys. Lett. **41**, 303 (1998).
- ¹⁴¹M. Conti, Y. Bustanji, G. Falini, P. Ferruti, S. Stefoni, and B. Samori, ChemPhysChem **2**, 610 (2001).
- ¹⁴²R. W. Tillmann, M. Radmacher, and H. E. Gaub, Appl. Phys. Lett. **60**, 3111 (1992).
- ¹⁴³M. Ludwig, W. Dettmann, and H. E. Gaub, Biophys. J. **72**, 445 (1997).
- ¹⁴⁴S. Manne, J. P. Cleveland, H. E. Gaub, G. D. Stucky, and P. K. Hansma, Langmuir **10**, 4409 (1994).
- ¹⁴⁵C. Möller, M. Allen, V. Elings, A. Engel, and D. Müller, Biophys. J. **77**, 1150 (1999).
- ¹⁴⁶J. P. Cleveland, S. Manne, D. Bocek, and P. K. Hansma, Rev. Sci. Instrum. **64**, 403 (1993).
- ¹⁴⁷H.-J. Butt and M. Jaschke, Nanotechnology **6**, 1 (1995).
- ¹⁴⁸F. Oesterhelt, M. Rief, and H. E. Gaub, New J. Phys. **1**, 6.1 (1999).
- ¹⁴⁹D. Y. C. Chan and R. G. Horn, J. Chem. Phys. **83**, 5311 (1985).
- ¹⁵⁰M. B. Viani, T. E. Schaffer, A. Chand, M. Rief, H. E. Gaub, and P. K. Hansma, J. Appl. Phys. **86**, 2258 (1999).
- ¹⁵¹A. F. Oberhauser, P. K. Hansma, M. Carrion-Vazquez, and J. M. Fernandez, Proc. Natl. Acad. Sci. U.S.A. **98**, 468 (2001).
- ¹⁵²J. V. Macpherson and P. R. Unwin, Anal. Chem. **72**, 276 (2000).
- ¹⁵³C. E. Jones, J. V. Macpherson, and P. R. Unwin, J. Phys. Chem. B **104**, 2351 (2000).
- ¹⁵⁴J. V. Macpherson and P. R. Unwin, Anal. Chem. **73**, 550 (2001).
- ¹⁵⁵T. Hugel, N. B. Holland, A. Cattani, L. Moroder, M. Seitz, and H. E. Gaub, Science **296**, 1103 (2002).
- ¹⁵⁶N. B. Holland, T. Hugel, G. Neuert, D. Oesterhelt, L. Moroder, M. Seitz, and H. E. Gaub, Macromolecules **36**, 2015 (2003).
- ¹⁵⁷A. Serr and R. R. Netz, Europhys. Lett. (in press, 2005).
- ¹⁵⁸B. Haupt, J. Ennis, and E. M. Sevick, Langmuir **15**, 3886 (1999).
- ¹⁵⁹C. Friedsam, A. K. Wehle, F. Khner, and H. E. Gaub, J. Phys.: Condens. Matter **15**, S1709 (2003).
- ¹⁶⁰S. Løefas, B. Johnsson, A. Edström, S. Hansson, G. Lindquist, R.-H. Müller-Hillgren, and L. Stigh, Biosens. Bioelectron. **10**, 813 (1995).
- ¹⁶¹J. E. Butler, L. Ni, R. Nessler, K. S. Joshi, M. Suter, B. Rosenberg, J. Chang, W. R. Brown, and L. A. Cantarero, J. Immunol. Methods **150**, 77 (1992).
- ¹⁶²J.-Y. Shao and R. M. Hochmuth, Biophys. J. **77**, 587 (1999).
- ¹⁶³L. Schmitt, C. Dietrich, and R. Tampe, J. Am. Chem. Soc. **116**, 8485 (1994).
- ¹⁶⁴C. M. Kacher, I. K. Weiss, R. J. Stewart, C. F. Schmidt, P. K. Hansma, M. Radmacher, and M. Fritz, Eur. Biophys. J. **28**, 611 (2000).
- ¹⁶⁵P. Silberzan, L. Leger, D. Ausserre, and J. J. Benattar, Langmuir **7**, 1647 (1991).
- ¹⁶⁶A. Barrat, P. Silberzan, L. Bourdieu, and D. Chatenay, Europhys. Lett. **20**, 633 (1992).
- ¹⁶⁷C. T. Tripp and M. L. Hair, Langmuir **8**, 1120 (1992).
- ¹⁶⁸D. L. Angst and G. W. Simmons, Langmuir **7**, 2236 (1991).
- ¹⁶⁹A. Ulman, Chem. Rev. (Washington, D.C.) **96**, 1533 (1996).
- ¹⁷⁰R. G. Nuzzo and D. L. Allara, J. Am. Chem. Soc. **105**, 4481 (1983).
- ¹⁷¹G. M. Whitesides and P. E. Laibinis, Langmuir **6**, 87 (1990).
- ¹⁷²L. H. Dubois and R. G. Nuzzo, Annu. Rev. Phys. Chem. **43**, 437 (1992).
- ¹⁷³C. Friedsam, A. del Campo Bcares, U. Jonas, H. E. Gaub, and M. Seitz, ChemPhysChem **5**, 388 (2004).
- ¹⁷⁴C. Friedsam, A. del Campo Bcares, U. Jonas, M. Seitz, and H. E. Gaub, New J. Phys. **6**, 9 (2004).
- ¹⁷⁵R. Schweiss, P. B. Welzel, C. Werner, and W. Knoll, Langmuir **17**, 4304 (2001).
- ¹⁷⁶C. Friedsam, H. E. Gaub, and R. R. Netz, Europhys. Lett. (in press).
- ¹⁷⁷S. S. Shiratori and M. F. Rubner, Macromolecules **33**, 4213 (2000).
- ¹⁷⁸F. Bordini *et al.*, Macromolecules **35**, 7031 (2002).
- ¹⁷⁹G. Koper and M. Borkovec, J. Phys. Chem. B **105**, 6666 (2001).
- ¹⁸⁰Y. Burak and R. R. Netz, J. Phys. Chem. B **108**, 4840 (2004).
- ¹⁸¹A. F. Xie and S. Granick, Nat. Mater. **1**, 129 (2002).
- ¹⁸²H. J. Kreuzer, R. L. C. Wang, and M. Grunze, J. Am. Chem. Soc. **125**, 8384 (2003).
- ¹⁸³R. R. Netz, J. Phys.: Condens. Matter **15**, S239 (2003).
- ¹⁸⁴U. Jonas, A. del Campo, C. Krüger, G. Glasser, and D. Boos, PNAS **99**, 5034 (2002).
- ¹⁸⁵P. J. Flory, *Statistical Mechanics of Chain Molecules* (Hanser, Muenchen, 1988).
- ¹⁸⁶M. Doi and S. F. Edwards, *The Theory of Polymer Dynamics* (Oxford University Press, Oxford, 1998).
- ¹⁸⁷O. Kratky and G. Porod, Recl. Trav. Chim. Pays-Bas **68**, 1106 (1949).
- ¹⁸⁸C. Bustamante, J. F. Marko, E. D. Siggia, and S. Smith, Science **265**, 1599 (1994).
- ¹⁸⁹F. Oesterhelt, M. Rief, and H. E. Gaub, New J. Phys. **1**, 6.1 (1999).
- ¹⁹⁰J. F. Marko and E. D. Siggia, Macromolecules **28**, 8759 (1995).
- ¹⁹¹M. D. Wang, H. Yin, R. Landick, J. Gelles, and S. M. Block, Biophys. J. **72**, 1335 (1997).
- ¹⁹²D. W. Urry *et al.*, Philos. Trans. R. Soc. London, Ser. B **357**, 169 (2002).
- ¹⁹³L. Livadaru, R. R. Netz, and H. J. Kreuzer, Macromolecules **36**, 3732 (2003).
- ¹⁹⁴A. Lamura, T. W. Burkhardt, and G. Gompper, Phys. Rev. E **64**, 061801 (2001); C. Storm and P. C. Nelson, *ibid.* **67**, 051906 (2003).
- ¹⁹⁵H. J. Kreuzer and M. Grunze, Europhys. Lett. **55**, 640 (2001).
- ¹⁹⁶J. C. L. Hagemann, R. J. Meier, M. Heinemann, and R. A. de Groot, Macromolecules **30**, 5953 (1997).
- ¹⁹⁷F. Bartha, F. Bogar, A. Peeters, C. van Alsenoy, and V. van Doren, Phys. Rev. B **62**, 10142 (2000).
- ¹⁹⁸L. Livadaru, R. R. Netz, and H. J. Kreuzer, J. Chem. Phys. **118**, 1404 (2003).
- ¹⁹⁹T. Hugel, M. Rief, M. Seitz, H. E. Gaub, and R. R. Netz, Phys. Rev. Lett. **94**, 048301 (2005).
- ²⁰⁰M. W. Schmidt *et al.*, J. Comput. Chem. **14**, 1347 (1993).